Journal of Modern Applied Medical Sciences

Assessment and Treatment of Some Heavy Elements of Groundwater Wells in Karbala Province / Iraq

Hasan F. Alesary [1,2], Hani K. Ismail [3], Ahmed Al-Yasari [1,4], Safaa D. Shoiliya [5], Stephen Barton[6]

[1]College of Applied Medical Science, University of Kerbala, Karbala, Iraq.

[2] University of Leicester, Leicester, United Kingdom

[3]Department of Chemistry, Faculty of Science and Health, Koya University, Koya 44023, Kurdistan Region – F.R., Iraq.

[4]School of Chemistry, University of East Anglia, Norwich Research Park, Norwich, NR7 4TJ, UK

[5]Karbala Education Directorate, Karbala. Iraq.

[6]School of Life Sciences, Pharmacy and Chemistry, Kingston University London, Kingston-Upon-Thames KT1 1LQ, Surrey, U.K.

Abstract

This study focused on purifying well water from heavy metals, specifically targeting eleven samples collected from various locations within the holy city of Karbala. Concentrations of key heavy elements such as zinc, chromium, aluminum, copper, lead, and cadmium were measured using atomic absorption devices. Of note, the highest concentrations of lead, cadmium, and aluminum were found in the selected well water samples. CaFe2O4 nanoparticles were combined with graphene oxide (GO), and their distinctiveness was established through diagnostic methods including FTIR, TEM, XRD, and FESEM. These techniques confirmed the successful synthesis of CaFe2O4 graphene oxide nanoparticles, which exhibited remarkable efficacy in adsorbing heavy elements. The outcomes revealed that cadmium exhibited the highest adsorption rate when utilizing 5 mg of the prepared nanomaterial at a temperature of 20 °C, achieving an adsorption rate of 81.27. In the case of aluminum, the use of 5 mg of the nanomaterial at a temperature of 25 °C demonstrated an exceptional adsorption rate of 99.09Likewise, for lead, the highest adsorption rate was achieved by employing 4 mg of the nanomaterial at a temperature of 25 °C, yielding an adsorption rate of 88.50. Utilizing a sample size of 3 ml resulted in an adsorption rate of 91.09, while a reaction time of 1 hour demonstrated the highest rate of 91.65, illustrating the most effective adsorption conditions for lead. The GO/CaFe2O4 nanoparticle exhibited remarkable adsorption efficiency under various conditions, showing its potential in heavy metal removal from well water. This study highlights the successful utilization of graphene oxide nanomaterial for the purification of water.

Received: 07/01/2025 **Accepted**: 24/02/2025 **Published**:31/08/2025

Keywords: Detoxification, Heavy metals, Adsorption technique, Magnetic nanoparticles, Ground water

1. Introduction

Heavy metals have the potential to induce severe health issues, manifesting in various symptoms contingent on the type and quantity of metal ingested. Their toxicity mechanism involves the formation of complexes with proteins, wherein carboxylic acid (–COOH), amine (–NH2), and thiol (–SH) groups play a role. These altered biological molecules lose their normal functionality, leading to cellular dysfunction or death. Metal binding to these groups can deactivate crucial enzyme systems or disrupt protein structure, which is linked to the catalytic function of enzymes. Additionally, this form of toxin may trigger the generation of radicals-harmful chemicals responsible for the oxidation of biological molecules [1]. The prominent characteristics of non-biodegradability, toxicity, and the capacity for bioaccumulation of heavy metals have significant consequences for the presence, variety, and population of species within aquatic ecosystems. These metals, often referred to as trace elements due to their low concentrations in ecosystems, can exert a lasting impact. The contamination of water systems by heavy metals continues to worsen over time, driven by the increasing growth of the population and industrial development [2]. During the past three decades, with the advent of mining, the industrial revolution, and advancements in agriculture, heavy metal pollution has emerged as a significant threat to the environment, particularly to human life. This threat arises from the consumption of fish living in contaminated water, where elements such as lead (Pb), chromium (Cr), copper (Cu), and cadmium (Cd) undergo bioaccumulation through the food chain in aquatic ecosystems [3]. Heavy metals are naturally occurring and can also be found in industrial wastewater, leading to contamination concerns in both surface and groundwater. Numerous industries generate waste containing various heavy metals, which they discharge into the environment. The primary sources of heavy metal pollution include metal plating, mining, smelting, battery manufacturing, tanneries, petroleum refining, pigment production, printing, paint manufacturing, and the use of pesticides, among others.

The term "heavy metal" specifically refers to a category of metals (and metal-like elements) characterized by a density exceeding 5 g/cm³, atomic numbers exceeding 20, and toxicity or poisonous properties at low concentrations [4]. The presence of emerging pollutants is steadily rising in aquatic environments, while the availability of clean water is diminishing. By 2025, around half of the global population is projected to reside in regions facing water scarcity. This escalating challenge necessitates more complicated water remediation strategies to avert associated complications and toxic outcomes [5]. Nanotechnology offers the potential to conserve water and the finite energy resources linked to it, as well as to safeguard water and other vital natural resources from pollution. Furthermore, this approach could play a role in the protection of ecosystems, habitats, and biodiversity, ensuring the fulfillment of the needs of future generations. With the escalating public consciousness regarding environmental concerns, the escalating usage of harmful chemicals and solvents necessitates a shift towards eco-friendly strategies, making it no longer feasible to proceed without considering environmental sustainability [6]. Presently, reverse osmosis (RO) stands as the most efficient method for filtering heavy metal ions from water, utilizing deep RO filtration to purify wastewater effectively. However, RO equipment comes with a high cost, and treating 1 liter of wastewater requires 3 liters of tap water, leading to increased water resource consumption and the need for power equipment installation. Fiber filtration systems are effective for removing small particles and soluble salts from water. Adsorption, a method known for its effectiveness

in removing heavy metals, holds particular relevance in addressing water pollution and conducting water purification[7].Consequently, it is imperative to treat wastewater to separate heavy metals before its release into the environment. The application of membrane technology in wastewater treatment is not new. Membranes enable the removal of effluents that other technologies struggle to achieve. Membranes based on polyvinylidene fluoride (PVDF) have gained widespread use in scientific research and industrial processes, particularly in wastewater treatment. This is owing to their exceptional attributes such as strong chemical resistance, high thermal stability, and the ability to form membranes[8].

1.2 Graphene

Graphene and graphene oxide are composed of a single sheet of carbon atoms arranged in a honeycomb pattern, featuring a sequence of sp2 carbons and possessing a range of advantageous properties. The movement of massless electrons across the honeycomb lattice without scattering over a submicrometer distance grants nanographene a quantum confinement energy of approximately 1 eV, slightly higher than the standard temperature of 300 K [9]. Graphene oxide (GO) represents an oxidized variant of graphene with hydrophilic functional groups such as hydroxyl, carbonyl, and carboxyl groups, which must be (partially) reduced to ensure electrical conductivity. Microorganisms have the capability to reduce the oxygen-containing functional groups in nonconductive GO, resulting in biologically reduced bio-rGO. This forms a hydrogel containing closely connected microorganisms, extracellular polymeric substances, and conductive material particles [10]. Concerning biological wastewater treatment, it has been reported that graphene oxide can enhance ammonia removal by anammox bacteria [11]. Among the diverse graphenaceous compounds, GO finds frequent use in the electrodeposition of coatings containing graphene. Notably, one of the primary benefits of GO lies in its ability to disperse in water and other organic solvents [12]. Graphene materials, characterized by their lightweight and low-density nature along with a two-dimensional structure, have garnered interest among researchers for their application in absorbent materials designed for electromagnetic (EM) wave absorption [13]. Regrettably, the utilization of graphene sheets in composites or coatings is constrained because they do not uniformly disperse within the matrix, primarily owing to the absence of functional groups on their surface [14]. Graphene exhibits distinctive chemical and physical attributes encompassing optical, electrical, mechanical strength, and a substantial surface area, coupled with catalytic activity, rendering it potentially applicable in biomedicine for functions such as biosensors, cancer therapy, drug delivery, and antimicrobial activity [15].

1.3. Purification Techniques for Heavy Metals

The active remediation of soil heavy metal pollutants using the artificial freezing method has been a subject of limited scholarly investigation. Past experiments and theories have established that the dominant factor governing the efficacy of purification is the freezing rate adjacent to the freezing front [16]. Given the potential environmental ramifications of water purification systems, it becomes crucial to employ methodologies that assess and quantify these impacts. Life cycle assessment (LCA) is a method employed to appraise the environmental consequences of a product or service throughout its lifecycle [17]. In the domain of water and wastewater purification, a plethora of nanomaterials have been developed, encompassing polymer nanomaterials, carbon nanotubes, (nano) zeolites, carbon, graphene, metallic NPs, graphene quantum dots, and GO [18]. While reverse osmosis (RO) membranes exhibit the

ability to eliminate an array of substances from feed water, they often incorporate preliminary treatment steps to condition and adapt the feed water, thereby preventing membrane module clogging and fouling [19] Therefore, addressing the contamination of heavy metal ions in water is imperative to minimize its impact on human health. The efficiency of adsorption as a straightforward and cost-efficient technique for large-scale pollutant removal from water, such as in industrial wastewater treatment, has long been recognized [20]. An adsorbent can be defined as a material with high adsorption capacity, selectivity, rapid adsorption and desorption kinetics, and low energy consumption for regeneration, used to eliminate heavy metals [21]. Adsorption-based methods represent a cost-effective, adaptable, environmentally friendly approach for wastewater purification [22]

2. Materials and Methods

2.1. Chemicals and Reagents

The chemicals used in this study, which were graphene oxide, GO with a molar mass of 56 g/mol and Fe2O4, with a molar mass of 175.68 g/mol, and HCL with a molar mass of 36.5 g/mol, and cobalt with a molar mass of 60 g/ m, and aniline per sulfate PAS with a molar mass of 189.19 g/mol , and polyaniline PAI , and FeCl3 with a molar mass 162.34 g/mol, were purchased from Sigma Aldridge Company, Germany. The atomic absorption spectrophotometer standards for elements: Lead (Pb), Cadmium (Cd), Aluminum (Al), Cobalt (Co), Chromium (Cr), Zinc (Zn), Cupper (Cu) were obtained from SHEMADHZU, Japan.

2.2. Sample collection

Samples of contaminated water were collected from 11 different sources of well water, specifically from Karbala Governorate in central Iraq, and they were named for different places, for example, from the city center in Al-Nasr neighborhood and the south of the province through the land pilgrimage road, as well as from the wells of the farms on the Najaf road and also from the Milad neighborhood. The water samples were kept at room temperature for the next use either for direct measurement of heavy metal concentration or treated with composite nanomaterials.

2.3. Characterization

Fourier Transform Infrared Spectroscopy (FTIR) was employed to identify the major functional groups within the samples, utilizing an FT-IR Spectrometer, Spectrum Two, based in CT, USA. The morphology of the prepared materials was analyzed using Transmission Electron Microscopy (TEM) on a JEOL-2010 microscope operating at an accelerating voltage of 200 kV. Additionally, Field Emission Scanning Electron Microscopy (FESEM) was conducted using a JSM-6701F microscope from JEOL, activated at an accelerating voltage of 5 kV. Energy-Dispersive X-ray (EDX) elemental mapping was carried out on a JEOL JEM-ARF200F atomic resolution analyzer.

2.4. Preparation and Synthesis Methods

Poly aniline, graphene oxide CoFe2O4, and cheap nanomaterial were used. The synthesis process is summarized below:

2.4.1. Synthesis of Polyaniline/GO/$CaFe_2O_4$ Nanoparticles

CoFe2O4 nanoparticles were prepared via the hydrothermal process according to the literature. An aqueous solution of 5.4 g of FeCl3 6H2O (in 50 mL) and 2.38 g of CoCl2 6H2O (in 50 mL) were mixed in a molar ratio of 2:1, respectively, under ultrasonic irradiation for 30 min. Following this, a 3 M solution of NaOH was added dropwise to the salt mixture under constant stirring using a magnetic stirrer to increase the pH of the solution to 11–12. After that, the solution was heated at 80 C for 1 h. The mixture was then cooled at 25 C and the resultant black precipitate of CoFe2O4 was magnetically separated, washed with deionized water several times, and dried in a vacuum oven at 100 C overnight .[23]

Thereafter, the oxidant solution (APS) was slowly added dropwise from a separation funnel to the mixture of aniline-metal oxides placed in an

ice bath with magnetic stirring and a thermometer, as shown

Fig. 2.1. pictures of the polymerization process in the laboratory.

2.4.2. Synthesis of the Polyaniline Composite (PANI/GO/CoFe2O4)

composite was synthesized by chemical(polyaniline) polymerization monomer and 0.45 g of GO powder and

CoFe2O4 nanoparticles (the weight ratio of GO:CoFe2O4 was(1:1). Firstly, a fresh oxidant solution of APS was prepared in a molar ratio of 1.25:1 (oxidant to monomer) containing 1 M HCl solution. Secondly, 3 g of the polyaniline monomer was mixed with 0.45 g of GO:CoFe2O4 nanoparticles in a solution of 20 mL

HCl/100 mL deionized water in a 250 mL conical flask. The mixture was sonicated for 2 h and then placed on a magnetic hotplate with stirring at 50 C. 2 g of FeCl3 was then added to the solution (polyaniline + GO + CoFe2O4) as support agent and to enhance the polymerization process. Following by the addition dropwise of oxidant solution) of APS into the mixture to start the polymerization of the monomer. The polymerization process was carried out for 20 h at 50 C. The product was filtered using a Buchner funnel then washed with 500 mL of 0.3 M HCl, followed by pure deionized water until a clean solution of wastewater was obtained. Finally, the yield of wet polymer composite was placed into a vacuum oven overnight at 65 C to obtain dried polymer composite powder. The proposed reaction mechanism and structure for the synthesis of PANI/GO/ CoFe2O4 In case of preparation of pure

polyaniline, the polymer was prepared using a similar method to the above but in the absence of GO and CoFe2O4 nanoparticle.

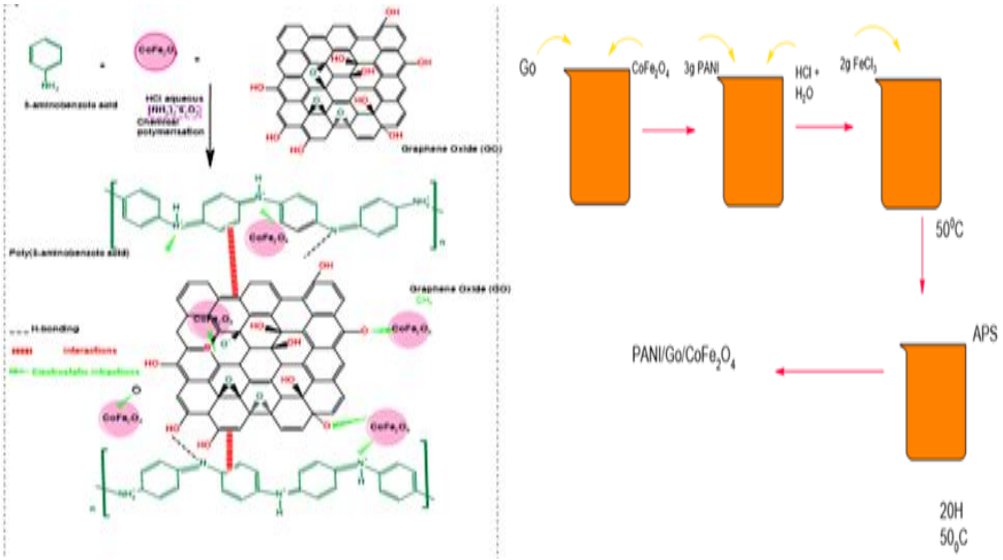

Fig.2.2. Synthesis of the polyaniline composite(PANI/GO/CoFe2O4)

2.4.3. Measurement of Element Concentration

The heavy metal concentrations were determined using the flameless (furnace) atomic absorption spectrophotometer technique. A suitable hollow cathode lamp (HCL) was employed for the analysis of each element under investigation (HCL lamp for Pb, HCL lamp for Cd, HCL lamp for Al, HCL lamp for Fe, HCL lamp for Co, HCL lamp for Cu, HCL lamp for Cr). In brief, the atomic absorption spectrophotometer was initially powered on for verification and allowed to heat for thirty minutes. Subsequently, water samples were directly injected into the furnace, where the samples were atomized according to a specific heating program. Following atomization, the temperature was gradually lowered to room temperature, and the absorbance was recorded and converted into concentrations using the processing unit of the AAS machine.

Fig. 2.3. Graphite (furnace) atomic absorption instruments the used in the measurement of the concentrations of elements.

2.5. Preparation of the Standard Solutions

Various concentrations (10 - 60 ppb) of working solutions were created from the stock standard solution for each element. The absorbance of these prepared solutions was gauged using an atomic absorption spectrophotometer with the graphite technique. Subsequently, the absorption values were transformed into concentrations using the Lambert-Beer law, as mentioned earlier. Following this, standard curves were constructed for each element and were employed to determine the concentration of unknown samples.

2.6. Adsorption of Heavy Metals by Synthesized Nanoparticles

Synthesized nanomaterials were employed to eliminate heavy metals from water samples through an adsorption technique. This method was utilized to remove heavy metals from selected samples with high concentrations (Al, Cd, Pb). The adsorption process following the addition of nanomaterials to the samples is depicted in Figure 2.4.

Fig. 2.4. Adding nanomaterial's to a sample of well water

3. Results and discussion

3.1. Characterization of PNAI/GO/CoFe2O4 Nanoparticles

The PANI/GO/Co Fe2O4 and PANI patterns were subjected to characterization through a range of techniques, including FTIR, XRD, SEM, TEM, For FTIR spectroscopy, polymer samples were blended with potassium bromide (KBr) powder and compressed to form transparent discs using a standard 13-mm disc compressor with a pressure of 30 tonnes. Spectra were acquired using a PerkinElmer Spectrum One Fourier Transform Infrared spectrophotometer (FTIR). A baseline KBr spectrum was recorded before capturing the spectra of any conducting polymer samples within the range of 400 to 4000 cm−1.The structural properties of the polymer composites were investigated using an X-ray diffractometer (Model: Panalytical Empyrean) operating at 45 kV, 30 mA, and scanned between 5° and 90° 20 with a step size of 0.02° 2θ, situated in the Department of Physics at Koya University. The surface morphology of the polymer nanocomposites was assessed using a Phillips XL30 Environmental Scanning Electron Microscope (ESEM) instrument with an acceleration voltage of 10 keV, as well as a Transmission Electron Microscope (TEM) PHILIPS CM120..The zeta potentials for PANI and PANI/CO/Fe2O4 nanocomposites were measured using a Malvern ZEN2600 Zetasizer in London, United Kingdom, across varying pH values (from 2 to 10). For sorption studies, sorbent doses of 0.1 g were mixed with 50 mL of 0.1 M KCl solution.

3.1.1. FT-IR Spectroscopy

FTIR analysis was conducted to characterize the functional groups present in the nanocomposite of PANI graphene oxide /$CoFe_2O_4$. The absorption spectra, illustrated in Figure (3.1), displayed distinct peaks at wave numbers of 500 and 510 cm^{-1}, corresponding to the extended vibrations of the (OH) group associated with FeOH. Additionally, a peak at 644 cm^{-1} was observed, indicative of the amide group (C=O). The presence of an (OH) extension was clearly depicted by a notable band at 3446 cm^{-1}, signifying the polyphenol group. Another significant band at 2928 cm^{-1} can be attributed to the expansion of (C-H) in the aldehyde functional group. Moreover, the peak at 1576 cm^{-1} indicated the bending of (C-H) in the aromatic compound, while the peaks at 1297 and 1114 cm^{-1} indicated the expansion of carbon dioxide.

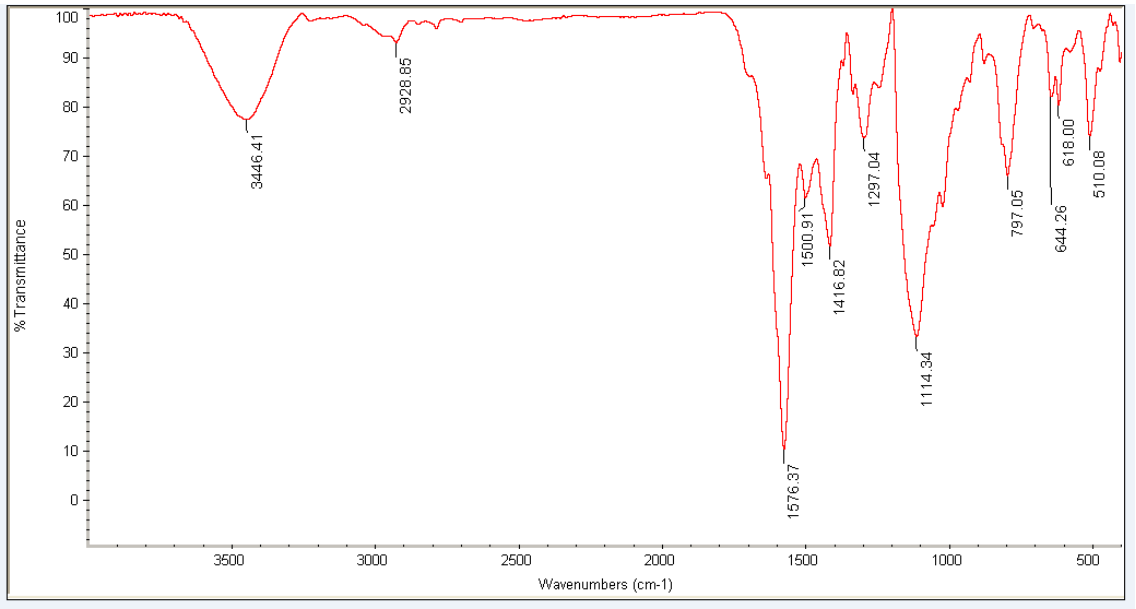

Fig. 3.1. FTIR Spectrum of Graphene Oxide CaOFe$_2$O$_3$

The figure 3.1 refers to the compound (PANI/GO/COFe$_2$O$_4$) which was prepared in the above paragraph 3.1 and under conditions and before adding it to the sample it was examined at FTIR. The findings reveal that graphene oxide encompasses a variety of functional groups, including phosphate, hydroxyl, amine, and carboxyl, which collectively contribute to the reduction of Fe$_2$O$_4$

3.1.2. Morphological and Structure Analysis

The elemental distribution of the prepared nanoparticles was examined by EDX-SEM to determine the elements. The shape of the particles was studied and its components were found to contain Fe, N, C, O, S, which are present in the PANI graphene oxide /CoFe2O4 nanoparticle as shown in Figure 3.2B.

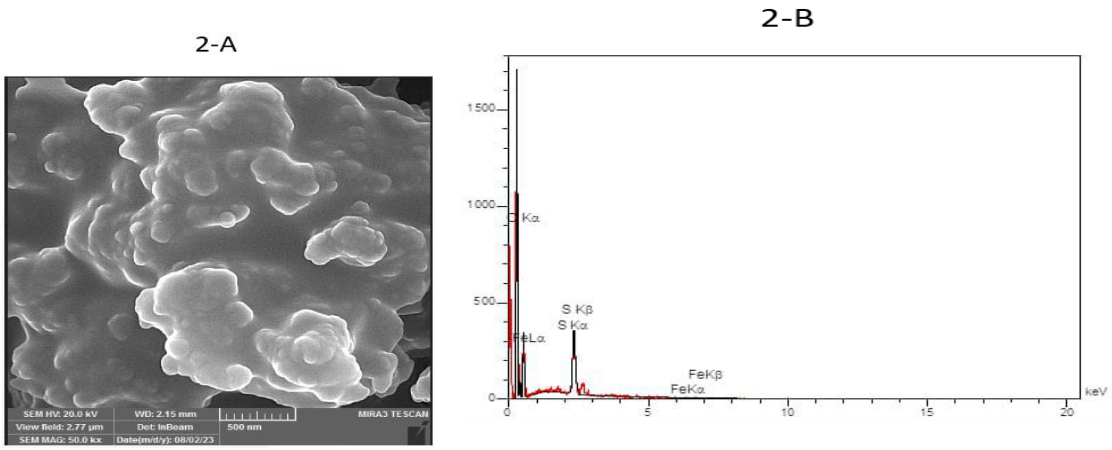

Fig. 3.2. (a) FESEM images of the as prepared of graphene oxide Caofe2o3 nanoparticles, (b) TEM image of graphene oxide CaOFe$_2$O$_3$.

3.1.3 EDX Analyses for PANI Polyaniline GO/CoFe2O4 Nano Particle

correspond to the strong interfacial interaction between GO and PANI with CoFe2O4, which indicates that the properties of magnetic CoFe2O4 were present in the PANI /GO/ CoFe2O4 Nano composite to some extent

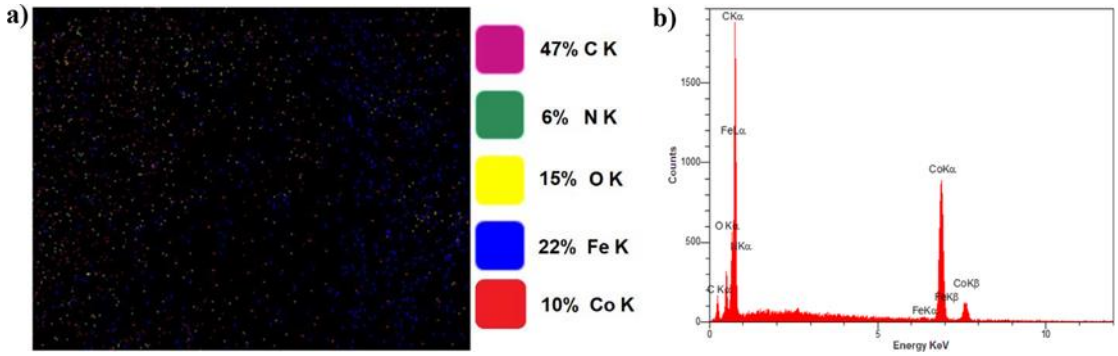

Fig.3.3.EDX images for a) elemental mapping, and b) peak line analysis of the PANI/GO/CoFe2O4 Nano composite

3.1.4. XRD Analysis

The X-ray diffraction (XRD) analysis of the synthesized PANI/GO/$COFe_2O_4$ is illustrated in Figure 3.4. The peaks observed in the XRD pattern are attributed to the inherent soft organic structure of graphene oxide, suggesting that the prepared nanomaterial is amorphous. These findings are consistent with the observations from TEM and FESEM images, indicating the clustering of $COFe_2O_4$ within the graphene oxide copolymers.

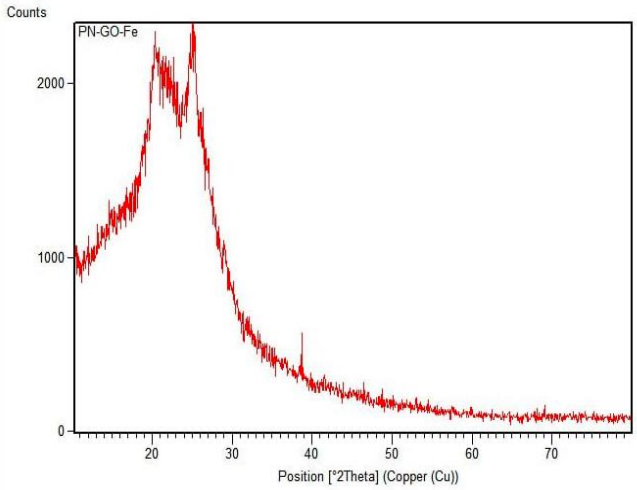

Fig. 3.4 XRD pattern of PANI/GO/$COFe_2O_4$ NPs

3.2. Measurement of Heavy Metals Concentration

The concentrations of heavy metals in the samples underwent assessment through a two-phase process using an atomic absorption device. The initial measurement was performed on the sample alone, followed by a second measurement after the introduction of the nanomaterial.

The newly developed dynamic beam manager system enables highly sensitive measurements. For flame measurements, typically a minimum of 1 mL (1000 µL) of solution is required, as the sample is continuously drawn into the system. However, the micro-sampling technique involves injecting only 50 to 100 µL of the sample into the flame at a time, facilitating quantification based on the height and area of the peak-shaped signal. Therefore, industrial effluents present a broad spectrum of environmental challenges, with increasingly complex and severe health risks. Photocatalytic degradation, a subset of advanced oxidation processes, has proven to be a highly efficient approach for antibiotic degradation (Tayyab et al., 2023a, 2023b). Within water, photocatalysts can break down organic pollutants into smaller, non-hazardous compounds through the generation of highly reactive groups, such as hydroxyl radicals. These reactive species are produced during photocatalytic reactions when exposed to light energy, water, and oxygen molecules [24].

3.3. Measurement of Elements Using Started Method

Eleven samples of well water were collected from various regions of the Holy Karbala. The concentrations of toxic elements were assessed both before and after introducing the nanomaterial's. Upon placing the samples into the device, and upon activating the device, the graphite furnace is prepared. The computer identifies the element to be measured, as well as the corresponding element's bulb within the device. The absorption device is positioned, and the concentration is recorded. This method is referred to as direct injection, where the sample is injected directly into the graphite furnace. However, in this direct injection method, only absorbance is measured. Through a specific equation provided by the device for each element, the absorbance is subsequently converted into concentration.

3.3.1. Standard method for measurement of Pb concentration

The lead element's concentration was determined and calculated using an atomic absorption device. To establish the calibration curves, a range of standard solutions for the lead element was prepared, with concentrations ranging from 10 to 60 ppb, as depicted in the calibration curve below.

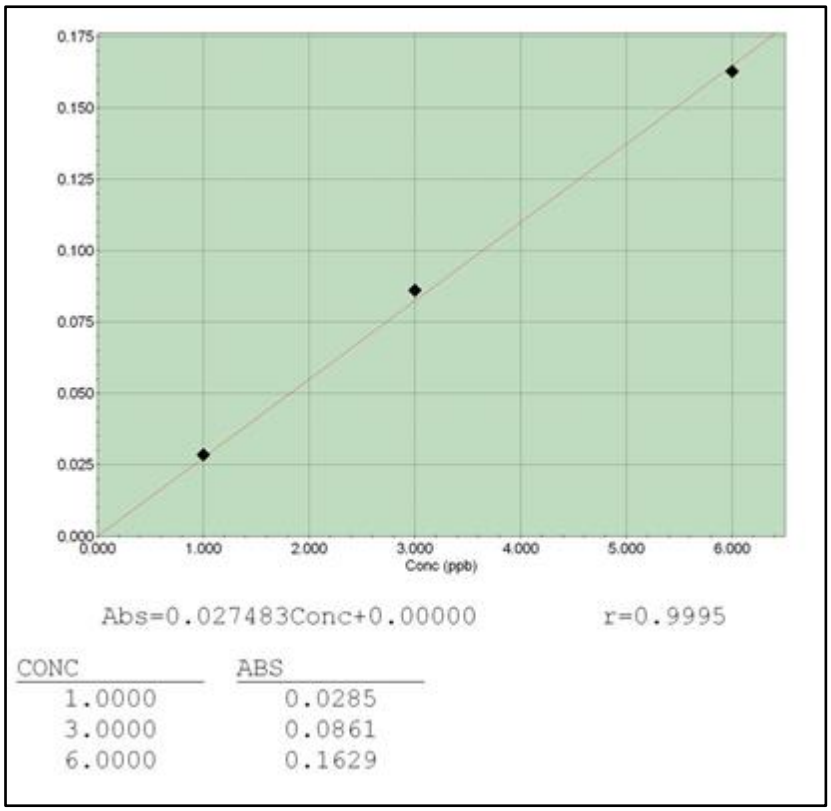

Fig. 3.5. Calibration Curve for Lead Determination

Depending on the standard curve in Figure (3.4), the Concentration of lead was measured in 11 samples.

Table 3.1. Operating conditions of the device for lead estimation.

Variable	Ideal condition
Lamp current	10 Ma
Wavelength	283.3nm
Slit width	0.7nm
Lighting mode	BGC-D2
Sample Volume	20 µl
Replicates	3

Table 3.1 shows the operational conditions for estimating the lead Concentration taken from the atomic absorption device.

Table (3.2). Measurement of Absorbance and Concentration of Lead

Sample	Conc. (ppb)	Abs.
1	445.9	12.254
2	751.3	20.647
3	533.1	14.651
4	1078.6	29.643
5	642.2	17.649
6	860.4	23.646
7	773.1	21.247
8	511.3	14.052
9	511.3	14.052
10	533.1	14.651
11	794.9	21.846

The lead concentration was assessed through an atomic absorption device, employing the automated approach. The analysis revealed that the highest lead concentration was present in sample No. 4, reaching 1078.6 ppb. Consequently, sample No. 4, originating from a well in Al-Nasr neighborhood within the holy city of Karbala, was chosen for further experimentation involving the addition of nanomaterials under varying conditions.

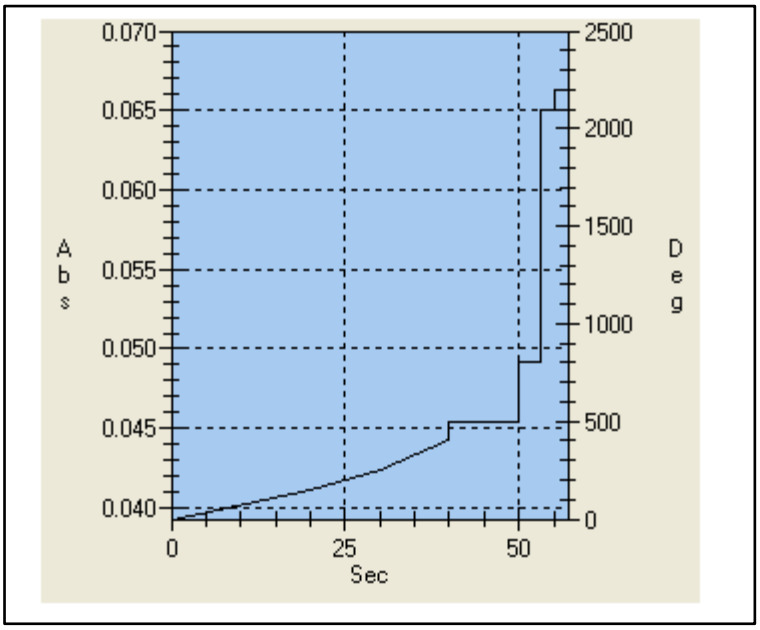

Fig. 3.6. Standard Lead Wavelength from an Atomic Absorption Device.

3.3.2. Stander method for Measurement of Cd Concentration

The cadmium concentration was determined using an atomic absorption device, involving the utilization of a series of standard solutions of the cadmium element, ranging from 10 to 60 ppb, for the calibration curves illustrated below. The calibration curve is presented as follows:

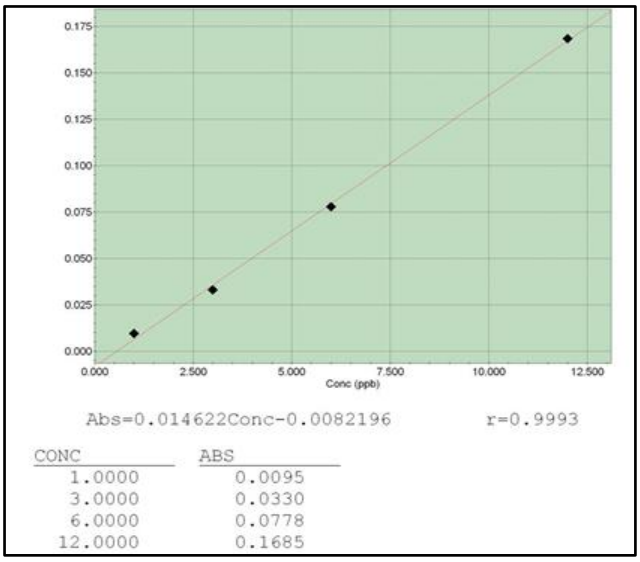

Fig. 3.7. Calibration curve for cadmium determination.

Depending on the calibration curve in Figure (3-6), the concentration of Cd was measured in 11 samples.

Table 3.3. Operating Conditions of the Device For Cadmium Estimation

Variable	Ideal condition
Lamp current	8Ma
Wavelength	228.8nm
Slit width	0.7nm
Lighting mode	BGC-D2
Sample Size	20 µl
Replicates	3

Table 3.3 shows the operational conditions for estimating the cadmium concentration taken from the atomic absorption device.

Table 3.4. Measurement of Absorbance and Concentration of Cadmium

Sample	Conc. (ppb)	Abs.
1	**12.4**	**1.8049**
2	**18.9**	**2.7553**
3	**11.1**	**1.6148**
4	**14.0**	**2.0388**
5	**16.0**	**2.3313**
6	**14.7**	**2.1412**
7	**14.0**	**2.0388**
8	**13.7**	**1.9949**
9	**18.2**	**2.6529**
10	**16.9**	**2.4628**
11	**26.7**	**3.8958**

The concentration of cadmium was determined utilizing an atomic absorption device and employing the automated method. It was observed that the sample with the highest cadmium concentration was sample No. 11 (26.7 ppb). Based on this observation, sample No. 11 was chosen for further testing, involving the addition of nanomaterials and varying experimental conditions. This particular sample was collected from a well in the Milad neighborhood within the sacred city of Karbala.

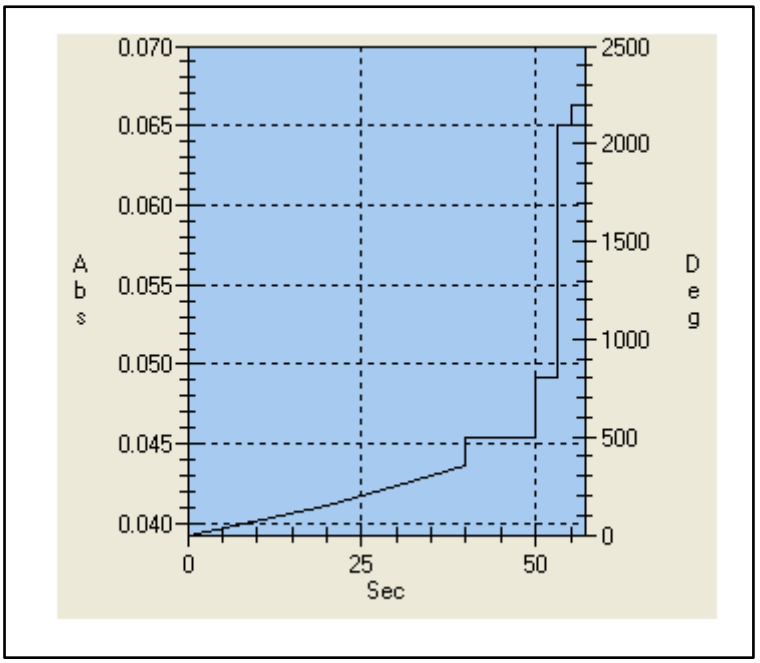

Fig. 3.8. Standard cadmium wavelength from an atomic absorption device.

3.3.3. Stander method for measurement of Al concentration

The concentration of the aluminum (Al) element was determined and assessed using an atomic absorption device. A set of standard solutions for the aluminum element was prepared, covering a range of concentrations (10 - 60 ppb), to establish the calibration curves as depicted below. Calibration curve illustrated below:

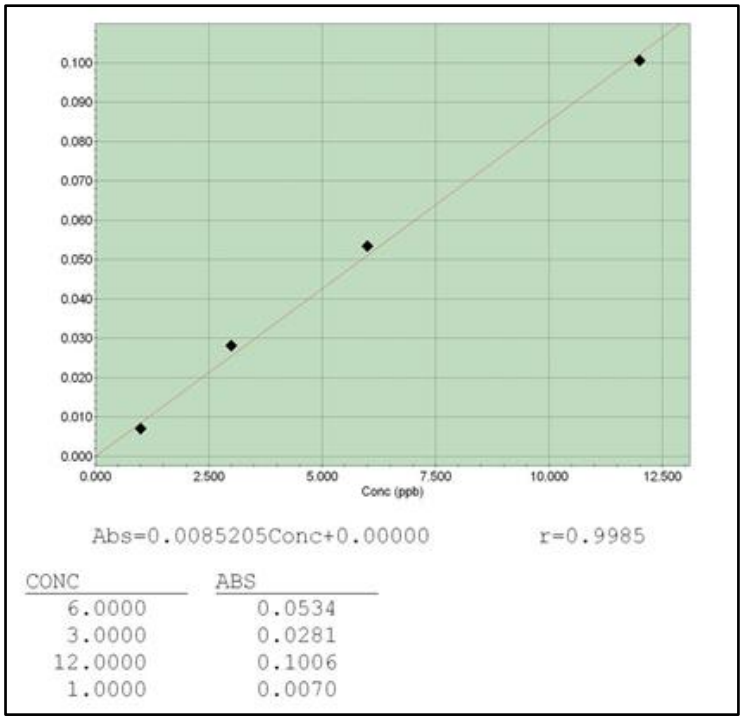

Fig. 3.9. Calibration Curve for Aluminum Determination

Depending on the calibration curve in Figure (3-8), the concentration of Al was measured in 11 samples using the instrumental conditions represented in Table 3.5. The obtained results are tabulated in Table 3.6.

Table 3.5. Operating Conditions of the Device for Aluminum Estimation

Variable	Ideal condition
Lamp current	10 ma
Wavelength	309.3 nm
Slit width	0.7 nm
Lighting mode	BGC-D2
Sample size	20
Replicates	3

Table 3.6. Measurement of Absorbance and Concentration of Aluminum

Sample	Conc. (ppb)	Abs.
1	**441**	**3.7575**
2	**261**	**2.2238**
3	**122**	**1.0395**
4	**104**	**0.8861**
5	**131**	**1.1161**
6	**81**	**0.6901**
7	**183**	**1.5592**
8	**74**	**0.6305**
9	**47**	**0.4004**
10	**123**	**1.0480**
11	**94**	**0.8009**

The concentration of aluminum was determined utilizing an atomic absorption device and the automated method. Notably, the highest aluminum concentration was observed in sample No. 1 (441 ppb). Consequently, sample No. 1 was chosen for further testing after the addition of nanomaterials and varying conditions. This sample was collected from one of the wells along the route to Najaf.

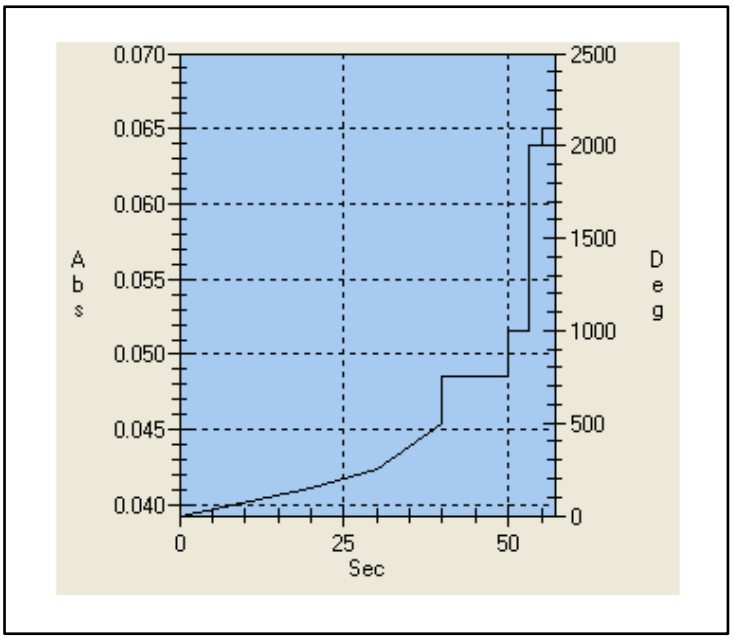

Fig. 3.10. Standard Aluminum Wavelength from an Atomic Absorption Device

3.3.4. Standard method for measurement of zinc concentration

The concentration of the Zn element was determined and estimated using an atomic absorption device. A set of standard solutions for the Zn element was prepared, covering a range of concentrations (10 - 60 ppb) for the calibration curves, as illustrated below. The calibration curve is shown in Figure 3.11.

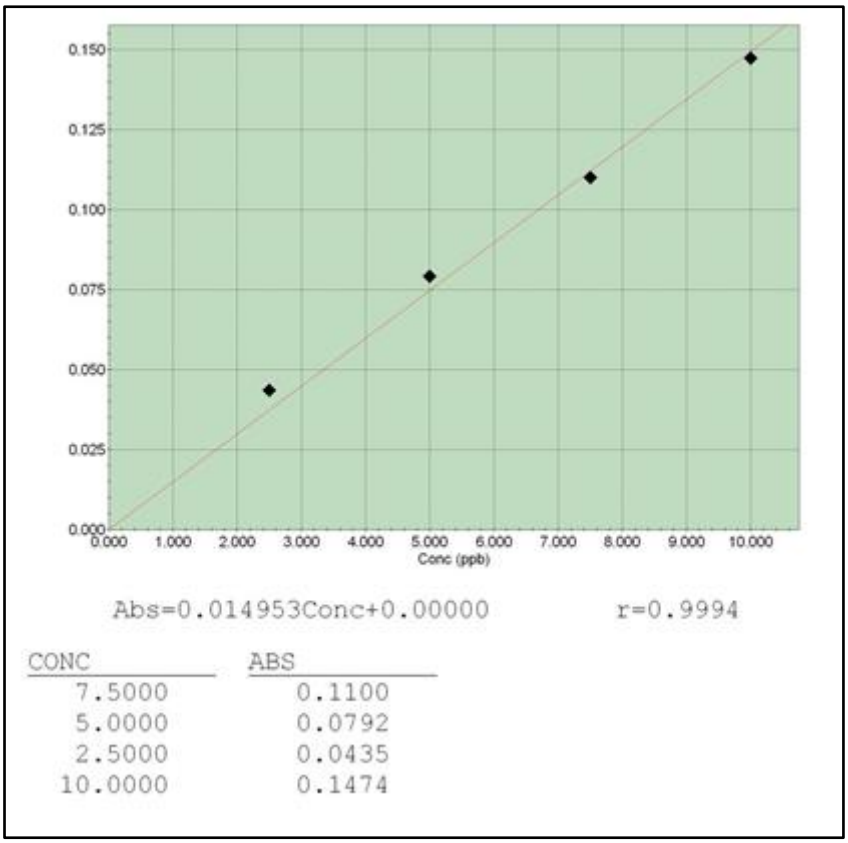

Fig. 3.11. Calibration Curve for Zinc Determination

Depending on the standard curve in Figure (3-10), the concentration of Zn was measured in 11 samples.

Table 3.7. Operating Conditions of the Device for Zinc Estimation

Variable	Ideal condition
Lamp current	8 mA
Wavelength	213.9
Slit width	0.7 nm
Lighting mode	BGC-D2
Sample size	20
Replicates	3

In this table shows the operational conditions for estimating the zinc concentration taken from the atomic absorption device.

Table 3.8. Measurement of Absorbance and Concentration of Zinc

Sample	Conc. (ppb)	Abs.
1	**58.8**	**0.8792**
2	**39.2**	**0.5861**
3	**54.4**	**0.8134**
4	**53.0**	**0.7925**
5	**54.2**	**0.8104**
6	**35.5**	**0.5308**
7	**26.3**	**0.3932**
8	**47.2**	**0.7057**
9	**31.9**	**0.4770**
10	**34.3**	**0.5128**
11	**1.8**	**0.0269**

The zinc concentration was measured using an atomic absorption device and using the automatic method, where it was noted that the highest concentration of zinc was in sample No. 1 (58.8 parts per billion) where this sample was taken from one of the wells on the Najaf road.

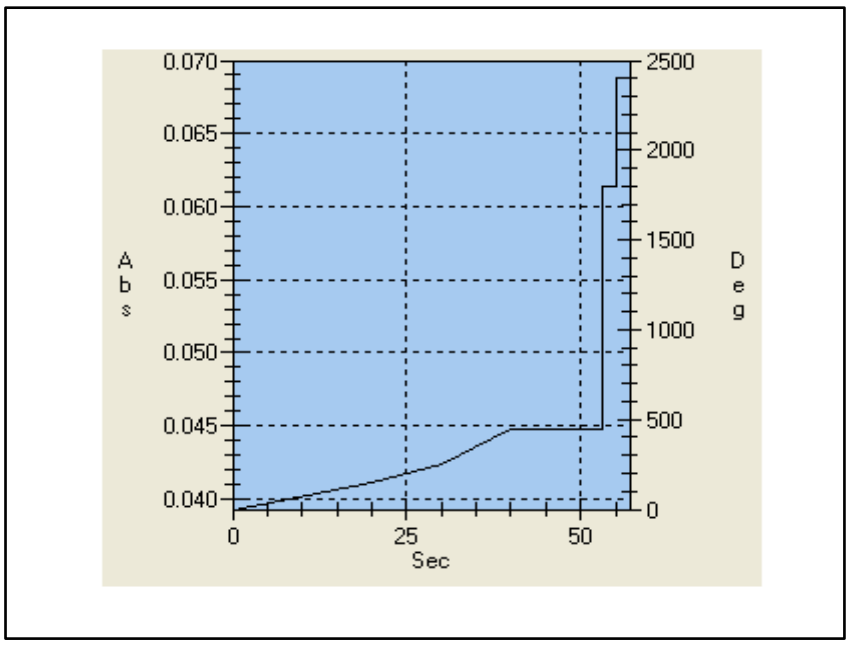

Fig. 3.12. Standard Zinc Wavelength from an Atomic Absorption Device

3.3.5. Standard Method for Measurement of Copper Concentration

Copper concentration was determined and estimated using an atomic absorption device. This involved the preparation of a range of standard solutions of the Cu element, spanning concentrations from 10 to 60 ppb. These solutions were employed to generate calibration curves, as illustrated below (Figure 3.13):

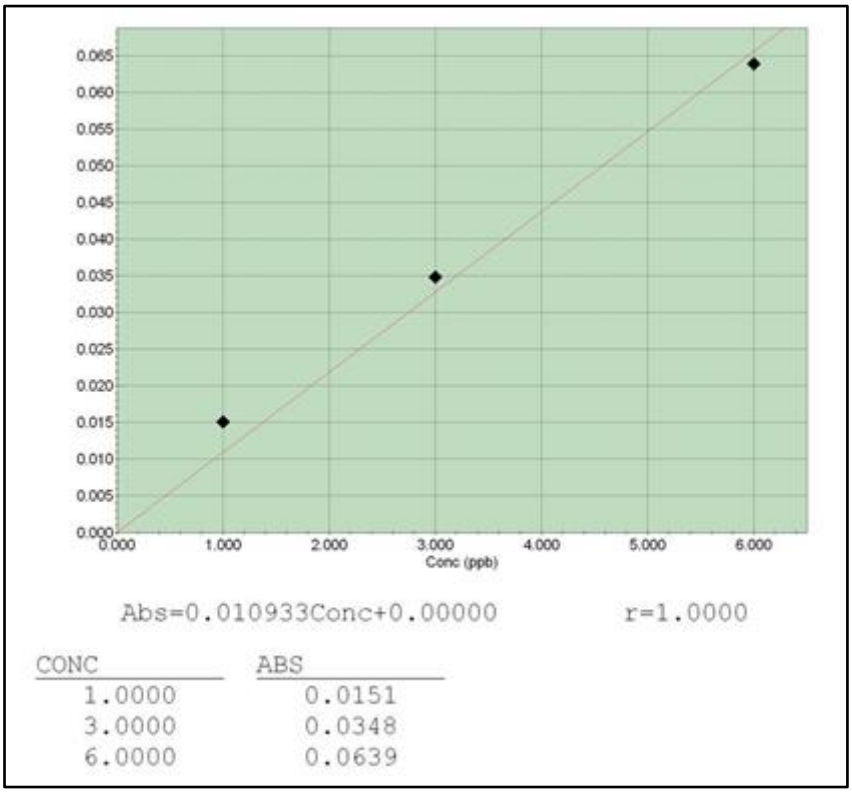

Fig. 3.13. Calibration Curve for Copper Determination

Depending on the standard curve in Figure (3-13), the concentration of Cu was measured in 11 samples using the condition tabulated in table 3.9, and the results are represented in Table 3.10.

Table 3.9. Operating Conditions of the Device for Copper Estimation

Variable	Ideal condition
Lamp current	6 mA
Wavelength	324.8
Slit width	0.7 nm
Lighting mode	BGC-D2
Sample size	20
Replicates	3

Table 3.10. Measurement of Absorbance and Concentration of Copper

Sample	Conc. (PPb)	Abs.
1	9.0	9.0983
2	11.8	0.1290
3	10.4	0.1137
4	11.8	0.1290
5	9.0	0.0983
6	20.2	0.2208
7	28.5	0.3115
8	16.7	0.1825
9	10.4	0.1137
10	7.0	0.0765
11	24.3	0.2656

The copper concentration was quantified using an atomic absorption device through an automated procedure. Notably, the highest copper concentration was observed in sample No. 11, registering at 24.3 ppb. This specific sample originated from a well located within the Milad neighborhood.

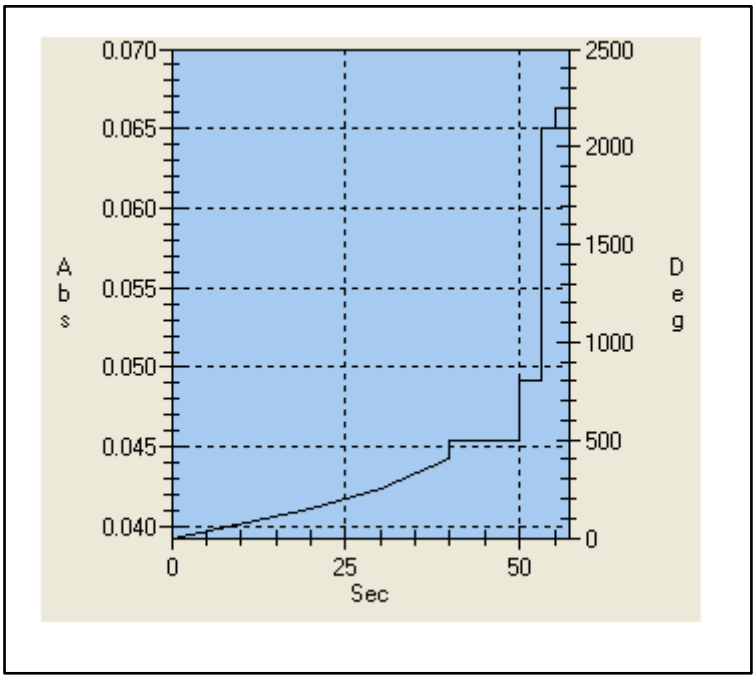

Fig. 3.14. Standard Copper Wavelength from an Atomic Absorption Device

3.3.6. Standard Method for Measurement of Chromium Concentration

The chromium (Cr) concentration was determined and estimated utilizing an atomic absorption device. A range of standard solutions for the Cr element was prepared, covering concentrations from 10 to 60 ppb. These solutions were used to construct calibration curves, as depicted below. Calibration curve is presented below for reference:

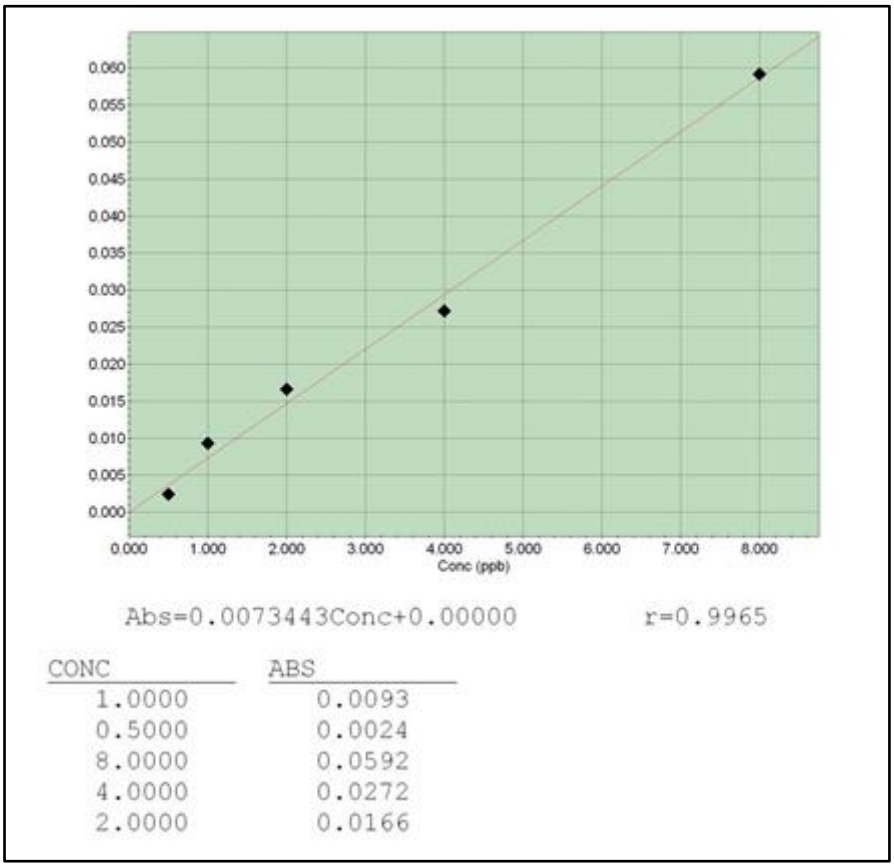

Fig. 3.15. Calibration Curve for Chromium Determination

Depending on the standard curve in Figure (3-15), the concentration of Cr was measured in 11 samples, and the results are tabulated in Table 3.12.

Table 3.11. Operating conditions of the device for chromium estimation

Variable	Ideal condition
Lamp current	10 mA
Wavelength	357.9 nm
Slit width	0.7 nm
Lighting mode	BGC-D2
Sample size	20
Replicates	3

In this table shows the operational conditions for estimating the chromium concentration taken from the atomic absorption device.

Table 3.12. Measurement of absorbance and concentration of chromium

Sample	Conc.(ppb)	Abs.
1	**8.2**	**0.06022**
2	**10.3**	**0.0756**
3	**6.4**	**0.0470**
4	**12.6**	**0.0925**
5	**7.4**	**0.0543**
6	**21.5**	**0.1579**
7	**22.6**	**0.1659**
8	**15.6**	**0.1145**
9	**10.1**	**0.07414**
10	**7.0**	**0.0514**
11	**21.4**	**0.1571**

Chromium concentration was assessed through an atomic absorption device employing the automatic method. Notably, the highest concentration of chromium was detected in sample No. 7, registering at 0.0016 ppb. This particular sample was collected from a well situated along the Pilgrimage road.

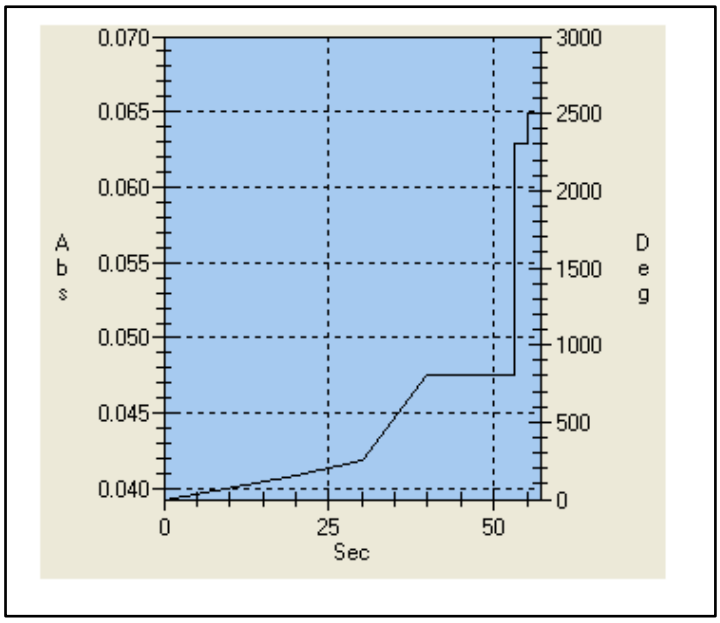

Fig. 3.16. Standard chromium wavelength from an atomic absorption device

3.4. Measurement of the concentration unknown sample

The prepared standard curves for each element served as the basis for analysis. The absorbance of the elements was measured, and their concentrations were determined using the slope equation corresponding to each element.

3.4.1. Measurement of lead

The concentration of lead was assessed using an atomic absorption device for the 11 samples under study. The outcomes revealed the lowest concentration in sample number 1, while the highest concentration was observed in sample number 4.Lead is a highly toxic heavy metal that can readily accumulate within the human body, leading to numerous health issues such as brain and kidney damage, as well as disruptions to the central nervous system, even at low concentrations Consequently, it is essential to engage in wastewater treatment to reduce the lead concentration in wastewater to levels below 0.02 mg/L in accordance with USEPA standards, ensuring a safe environment upon discharge. Various techniques, such as chemical precipitation, oxidation-reduction, coagulation-flocculation, ion exchange, and reverse osmosis, are commonly employed for the removal of heavy metals, including lead, from wastewater. Nevertheless, these methods come with drawbacks, including incomplete removal of heavy metals, high operational expenses, complex procedures, and the generation of substantial amounts of toxic sludge [25]. The acquired findings reveal a remarkably elevated concentration of this element. This heightened concentration has profound effects on organisms that rely on water with substantial lead content, spanning from humans to animals. Consequently, the imperative arises to decontaminate this freshwater from the element, necessitating the adoption of advanced, cost-effective, and environmentally benign purification technologies. Our research proposes such an approach, which will be elaborated upon in the subsequent sections.

3.4.2. Measurement of Cadmium

The cadmium concentration was measured using an atomic absorption device for the 11 studied samples, and the results were the lowest Concentration in sample no. (1) and the highest Concentration in sample no. (11). Currently, both field and laboratory research have provided insights into the ways in which silicon (Si) mitigates cadmium (Cd) toxicity and shields rice plants from Cd absorption. These effects primarily manifest in two key ways: Si acts as a passivating agent, reducing the activity of cadmium in the soil, or it hinders the migration and accumulation of cadmium within rice plants. An illustration of Si's impact can be observed when the soil's pH level is raised to 7 through Si application, resulting in a decrease in available Cd [26]. The obtained results reveal a significant elevation in the concentration of this element. Consequently, due to this heightened concentration, it exerts a notable influence on the organisms that rely on water with substantial cadmium content, encompassing both humans and animals. As a result, there arises a necessity to decontaminate this freshwater from the presence of cadmium, prompting the need for enhanced technological approaches. The subsequent discussion will delve into our research proposal, outlining efficient, cost-effective, and environmentally friendly methods for water purification that we have suggested.

3.4.3. Measurement of Aluminum

The concentration of aluminum was assessed utilizing an atomic absorption device across the 11 samples under investigation, yielding the lowest concentration in sample number (9) and the highest concentration in sample number (1). Particularly in developing countries, the release of aluminum from cookware reached levels of up to 125 mg per serving, surpassing WHO's recommended intake of 20 mg per day per person by more than sixfold. [27]. The obtained findings reveal a notably elevated concentration of this element. Due to its high presence, it exerts a substantial influence on organisms relying on water with a significant Aluminum content, encompassing both humans and animals. Consequently, the purification of this freshwater from the element becomes imperative, necessitating the application of advanced technologies. Our research proposes effective, cost-efficient, and environmentally benign methods for water purification, as elucidated in the subsequent discussion.

3.4.4. Measurement of Zinc

Utilizing an atomic absorption device, the zinc concentration was quantified across the 11 samples under investigation. The findings indicated the lowest concentration in sample number (11) and the highest concentration in sample number (1). Zinc is a vital element for aquatic organisms, yet its elevated concentrations can become toxic, especially in freshwater environments affected by urbanization, industrialization, and resource extraction. Water chemistry factors, including dissolved organic matter (DOM), pH, and hardness, play a crucial role in influencing metal toxicity. These parameters alter metal speciation and interactions at cellular surfaces, thus affecting their bioavailability [28]. The obtained results reveal a significant elevation in the Concentration of this element. Due to its high Concentration, it exerts an influence on organisms relying on water with substantial zinc content, including both

humans and animals. Consequently, the purification of such water from this element is imperative. Achieving this necessitates the utilization of advanced technologies that are efficient, cost-effective, and environmentally safe. Our research proposes solutions in this regard, which will be detailed in the subsequent sections.

3.4.5. Measurement of Copper

The Concentration of copper was determined using an atomic absorption device for the 11 samples under investigation. The outcomes indicated the lowest concentration in sample No. (10) and the highest Concentration in sample No. (7). Copper exhibits toxicity to phytoplankton by adversely affecting photosystem II. However, copper compounds could also impact non-target organisms, including the water flea which happens to be one of the most sensitive organisms to copper's effects [29]. The results obtained strongly underscore the notably high concentration of this element. This elevated concentration exerts a considerable influence on organisms depending on water with a substantial copper content, regardless of whether they are human or animal. As a result, the purification of such water from copper becomes imperative, requiring the application of advanced technology. We suggest that an efficient, cost-effective, and environmentally friendly approach can be implemented for water purification, as elucidated in our research findings, which will be elaborated upon in the subsequent discussion.

We can infer from the obtained results that the concentrations of the examined elements are indeed at concerning levels. Among these, the highest concentrations of three elements were chosen for treatment using the nanomaterial developed in our research.

3.4.6. Measurement of Chromium

Using an atomic absorption device, the chromium concentration was analyzed in the 11 investigated samples. The results indicated the lowest concentration in sample No. (3) and the highest concentration in sample No. (7). Cadmium, a toxic metal found in groundwater, typically occurs at low concentrations unless there is contamination from sources such as mining or industrial wastewater, or through leakage from hazardous waste sites. These contaminants can enter water sources through various pathways, including industrial processes, mining operations, and agricultural runoff [30]. The acquired findings demonstrate a notable increase in the levels of this element's concentration. Because of its elevated concentration, it impacts organisms that rely on water with substantial chromium content, encompassing both humans and animals. Consequently, the purification of such water from this element becomes essential. Accomplishing this requires the application of advanced technologies that are efficient, economically viable, and environmentally benign. Our research offers solutions in this context, elaborated in the subsequent sections.

3.5. Synthesis of Nanomaterial

Nanoparticles encompass diverse material categories with sizes less than 100 nm, categorized by material, dimension, and origin. Nanotechnology represents a multidisciplinary domain that

amalgamates biology, chemistry, medicine, physics, and materials engineering to create nanoscale structures. These structures display distinctive attributes like electronic, magnetic, and physicochemical properties, among others. Their significant surface area to volume ratio, crystallinity, and geometry contribute to these unique characteristics [31].

3.6. Purification of Heavy Metals by Ghraphene Oxide

Graphene oxide (GO)-based carbonaceous materials, derived from graphite, are commonly utilized as adsorbents for dye removal due to their unique 2-D structure characterized by interplanar distance, extensive surface area, robust mechanical and thermal properties, and several valuable functional groups including epoxy (- C A O A C), carboxyl (-COOH), hydroxyl (-OH), and hydrophilic groups. These functional groups enable GO to interact with diverse inorganic and organic compounds through covalent or non-covalent interactions, enhancing its ability to effectively adsorb cationic/anionic dyes and heavy metal ions [32]. Previous research has revealed that the adsorption process is a favorable approach for eliminating heavy metals from well water due to its favorable characteristics that do not have adverse effects on the water quality. Nevertheless, graphene oxide possesses certain limitations in the field of medicine owing to its elevated organ toxicity. Additionally, its presence of oxygen in a relatively high proportion hampers its electrochemical properties, diminishing electron mobility [33]. Graphene and graphene oxide are distinctive substances composed of a single sheet of carbon atoms arranged in a honeycomb pattern, featuring a chain of sp^2 carbons. These materials possess several beneficial characteristics. The unique honeycomb lattice structure allows massless electrons to traverse it over submicrometer distances without scattering, granting nanographene a quantum confinement energy of approximately 1 eV, slightly exceeding the temperature of 300 K [34].The electrochemical response is attributed to electron transfer between graphene and the adsorbed substances. When molecules adhere to the graphene surface, a charge transfer process occurs within the adsorption region. In this interaction, graphene can act as either a donor or acceptor, resulting in modifications to the carrier density, Fermi level, and electrical resistance of graphene. Over the past few decades, graphene has garnered significant interest in the realm of electroanalysis. It has become a focal point for the development of electrochemical monitoring devices designed to detect environmentally harmful and health-threatening substances like heavy metals, which pose risks to both the environment and human well-being [35]. To produce graphene in substantial quantities, an alternative technique is necessary, and one such method is chemical oxidation. In this process, functional groups like carbonyl, hydroxyl, and peroxyl are initially introduced between the carbon layers of graphite, resulting in the creation of graphene. These functional groups weaken the van der Waals bonds between the carbon layers, thereby causing the graphene layers to separate from the graphite material layer by layer [36].

3.6.1. Adsorption of Aluminum

These circumstances will ultimately result in substantial hardships, including both personal and financial costs, for families and society as a whole. This is particularly evident in developing countries, where the release of aluminum from cookware can reach levels as high as 125 mg

per serving, exceeding the World Health Organization's recommended daily intake by over sixfold (20 mg per day per person).

Aluminum contamination and associated inflammation represent an escalating public health concern. Investigating aluminum-induced immunotoxicity and elucidating potential underlying mechanisms warrant considerable attention [37]. Back in 1926, Glenny and colleagues were the first to demonstrate that the precipitation of insoluble aluminum salts could boost the immunogenicity of diphtheria toxoid. Following this discovery, aluminum adjuvants have frequently been employed to enhance the immune response in human vaccine formulations. Among the three aluminum adjuvants commonly found in licensed vaccines are aluminum hydroxide (AH), aluminum phosphate (AP), and amorphous aluminum hydroxyphosphate sulfate (AAHS) [38]. In our study, we focused on the adsorption of aluminum from water, driven by its elevated Concentration. The highest concentration was selected to address the purification objective. We employed optimal conditions and blended the nanomaterials with varying Concentrations and exposure durations. The duration was set at 15 minutes, the sample volume at 3 ml, and diverse temperatures were tested. The efficiency of bead removal was assessed by calculating the difference between the initial and final concentrations using the equation:

$$\text{Removal efficiency (\%)} = \frac{(ci - ct).100}{ci}$$

To determine the amount of metal adsorbed by the biosynthesized $CaFe_2O_4$-graphene oxide-NPs alginate beads (metal/adsorbent, mg/g), the calculation involved utilizing the initial concentration of lead (Ci, mg/L) and the concentration of lead at a specific time (Ct, mg/L) [39].

Table 3.13. The temperatures are different of aluminum

Temperatures (^{0}C)	Conc.(ppb) before treatment	Conc.(ppb) After treatment	Separation efficiency (%)
20	441	223	49.43
25	441	4	99.09
35	441	161	63.49
40	441	185	58.04

The experiments conducted in this study reveal that the most favorable temperature for efficient adsorption is 25 degrees Celsius. At this temperature, the concentration was reduced to 4 ppb, indicating a notably rapid adsorption rate and underscoring the efficacy of the employed nanomaterials in our research. Additionally, a set of experiments was carried out at a constant temperature of 25 degrees Celsius, using a sample size of 3, while altering the reaction time.

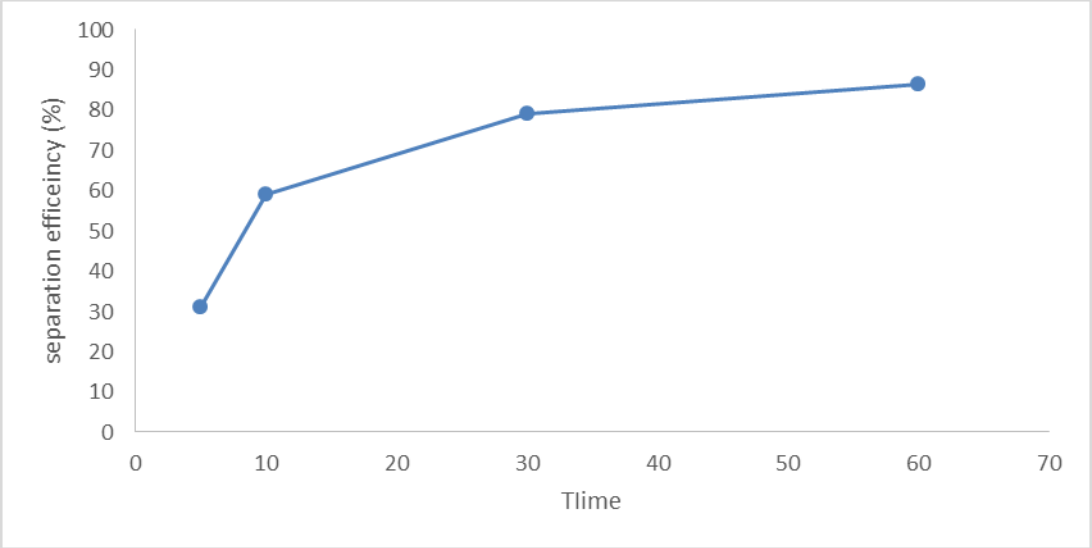

Figure 3.17. The effect of temperature on aluminum adsorption

Table 3.14. The effect of contact time on the removal percentage of Al(III)

Reaction time	Conc.(ppb) before treatment	Conc.(ppb) After treatment	Separation efficiency (%)
5 min	441	304	31.06
10 min	441	180	59.18
30 min	441	92	79.13
1 h	441	60	86.39

The findings from the above-mentioned experiments demonstrate that extending the reaction time enhances the absorption process. Notably, a positive outcome was attained with a complete hour of reaction, leading to a concentration decrease to 60 ppb. This outcome emphasizes the effectiveness of the utilized nanomaterial. Furthermore, a series of experiments were carried out under conditions of 25°C and a reaction time of 1 hour, with variations in the sample size.

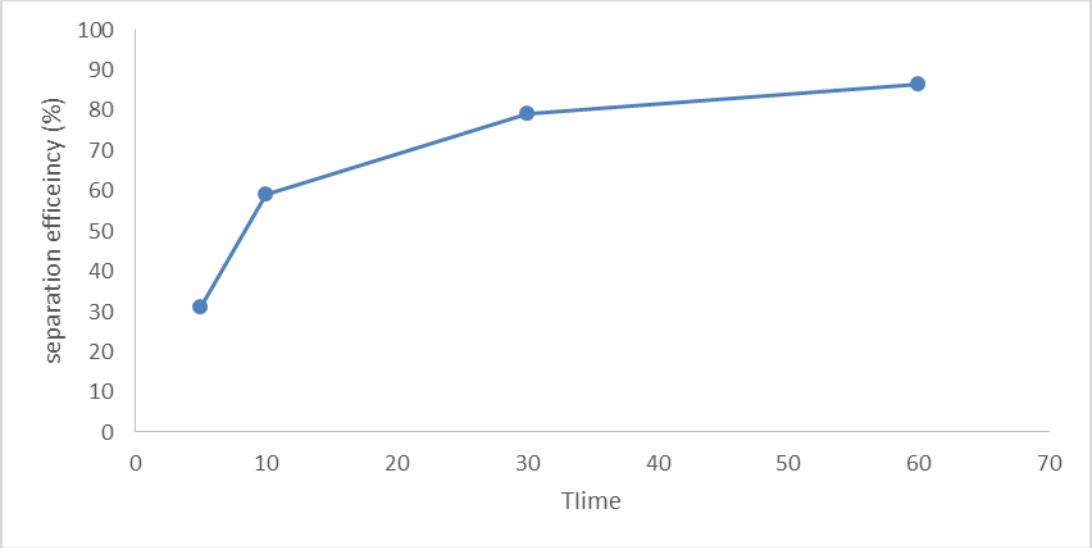

Fig. 3.18. The effect of reaction time on aluminum adsorption

Table 3.15. The effect of sample volume on the removal of Al(III)

Size (mL)	Conc.(ppb) before treatment	Conc.(ppb)After treatment	Separation efficiency (%)
3	441	68	84.58
4	441	154	75.07
5	441	34	92.29

As seen in the earlier experiments, the sample size influences the rate of adsorption. Notably, larger sample sizes lead to diminished adsorption effects. It's important to note that across all the mentioned experiments, a constant quantity of 5 mg of nanoparticles was utilized for the adsorption process. Drawing from the extensive experimental data, it can be deduced that the optimal conditions for the adsorption process are a temperature of 25°C, a reaction time of 1 hour, and a sample volume of 5 mL.

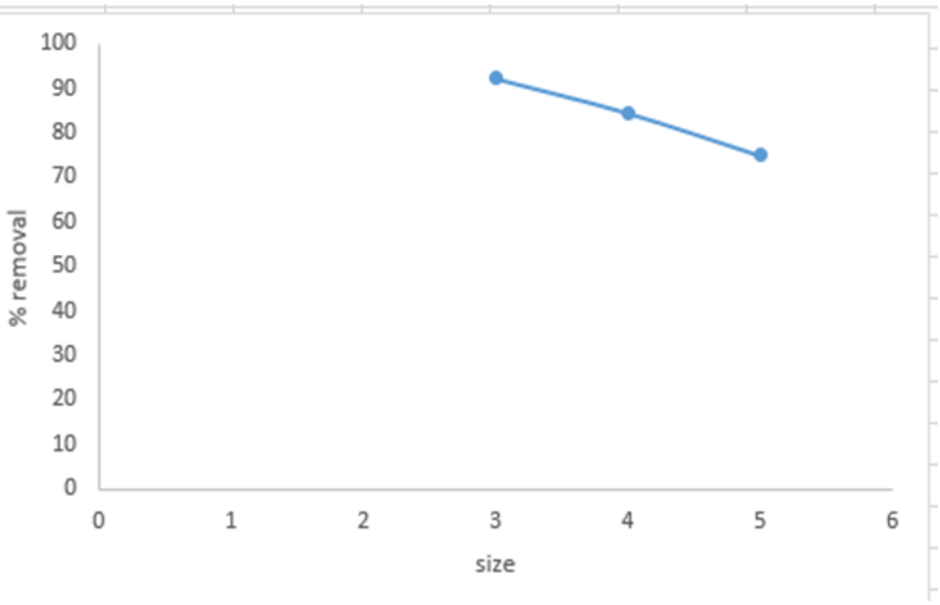

Fig.3.19. Graph showing the effect of size on aluminum adsorption.

3.6.2. Adsorption of lead

Hence, in order to achieve a safe environment, it is imperative to treat wastewater to reduce lead concentration below 0.02 mg/L in accordance with USEPA regulations. Numerous techniques such as chemical precipitation, oxidation-reduction, coagulation-flocculation, ion exchange, and reverse osmosis are commonly employed for removing heavy metals, including lead, from wastewater. Nonetheless, these methods have drawbacks such as incomplete removal of heavy metals, high operational expenses, intricate procedures, and the generation of substantial amounts of toxic sludge [40]. Nonetheless, adsorption has demonstrated itself as a straightforward and cost-efficient approach in wastewater treatment, with granular activated carbon being a commonly employed adsorbent. Adsorption can be conducted in both batch and continuous modes. While batch adsorption experiments are crucial for obtaining fundamental data on the removal of specific pollutants, continuous adsorption studies are essential for the practical application of this process in wastewater treatment [41]. Lead was selected due to its elevated concentration in the measured samples and its impact on drinking water and living organisms. The highest concentration was specifically chosen to facilitate purification. The ideal conditions were applied, and the nanomaterial was introduced into thesystem. A sample volume of 3 ml and a reaction time of 10 minutes were employed, along with variations in temperature.

Table 3.16. The temperatures are different of lead.

Temperatures °C	Conc.(ppb) before treatment	Conc.(ppb) Aftertreatment	Removal efficiency(%)
20	1078.6	157	85.44
25	1078.6	124	88.50
30	1078.6	485	55.03
35	1078.6	412	61.80

The conducted experiments reveal that the most efficient absorption process occurs at a temperature of 25 degrees Celsius. This substantiates the effectiveness of the nanomaterial, as the lead absorption from the sample proceeded at a notably rapid rate.

Furthermore, a series of experiments were conducted at a temperature of 25°C, employing a sample volume of 3 ml and varying the reaction time.

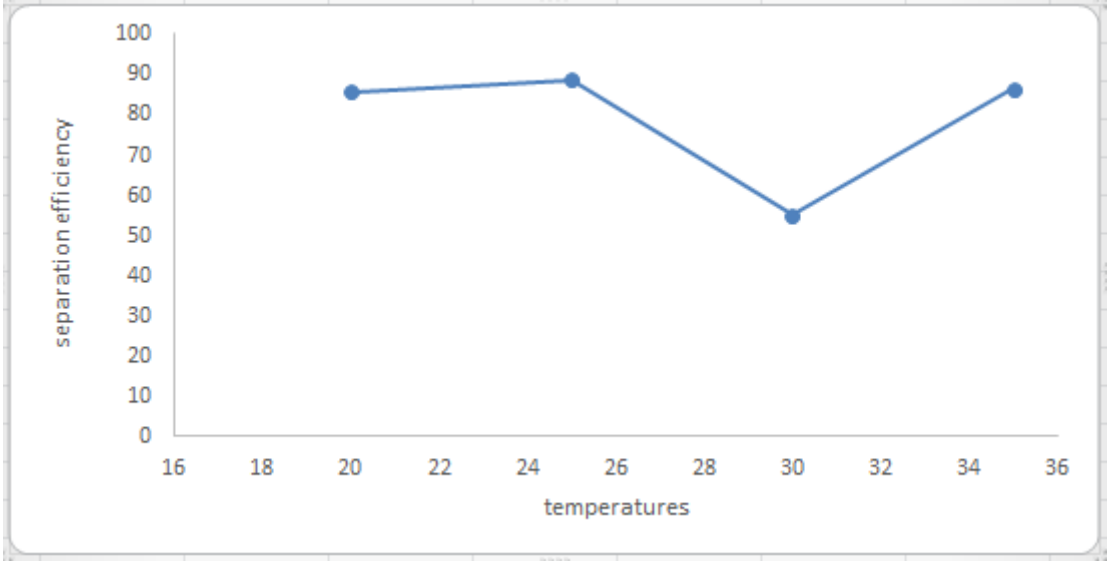

Fig. 3.20. The effect of temperature on lead adsorption

Table 3.17. The effect of contact time

Contact time	Conc.(ppb) before treatment	Conc. (ppb) Aftertreatment	Removal (%)
5 min	1078.6	710	34.17
10 min	1078.6	689	36.12
30 min	1078.6	106	90.17
1 hr.	1078.6	90	91.65

By examining the experiments presented in the table above, it becomes evident that favorable outcomes emerge as the reaction time is extended. This phenomenon highlights the efficacy of the nanomaterials used in this research, with a particularly notable result achieved at a reaction time of 1 hour, which is considered optimal for this study. Several experiments were also undertaken, maintaining a temperature of 25 °C, a duration of 1 hour, while varying the size of the sample.

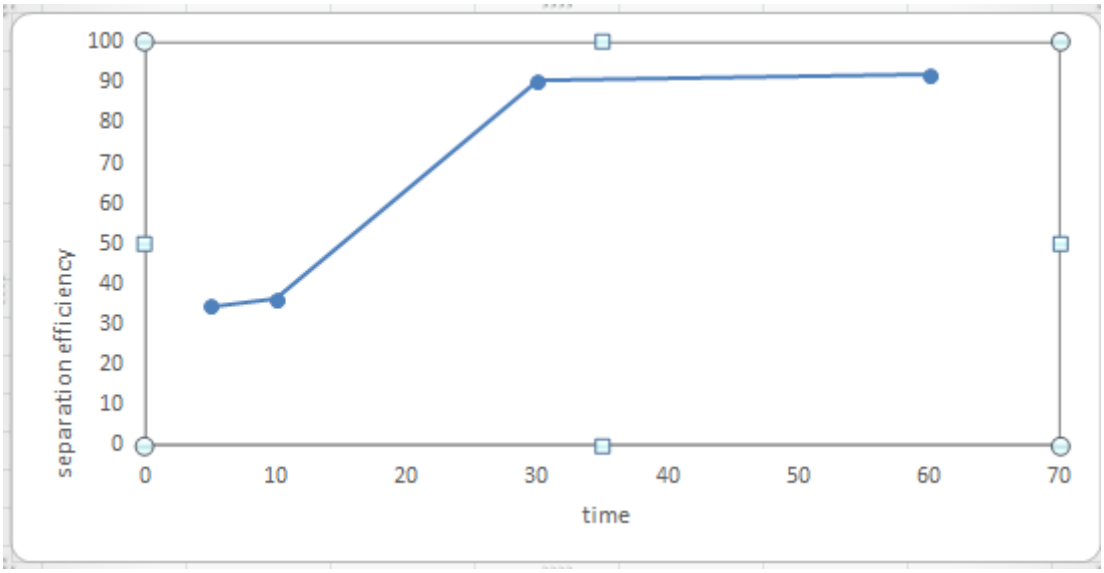

Fig. 3.21. The effect of reaction time on lead adsorption

Table 3.18. The effect of sample volume

Size(mL)	Conc.(ppb) beforetreatment	Conc.(ppb) After treatment	Removal efficiency(%)
3	1078.6	96	91.09
4	1078.6	110	89.80
5	1078.6	525	51.32

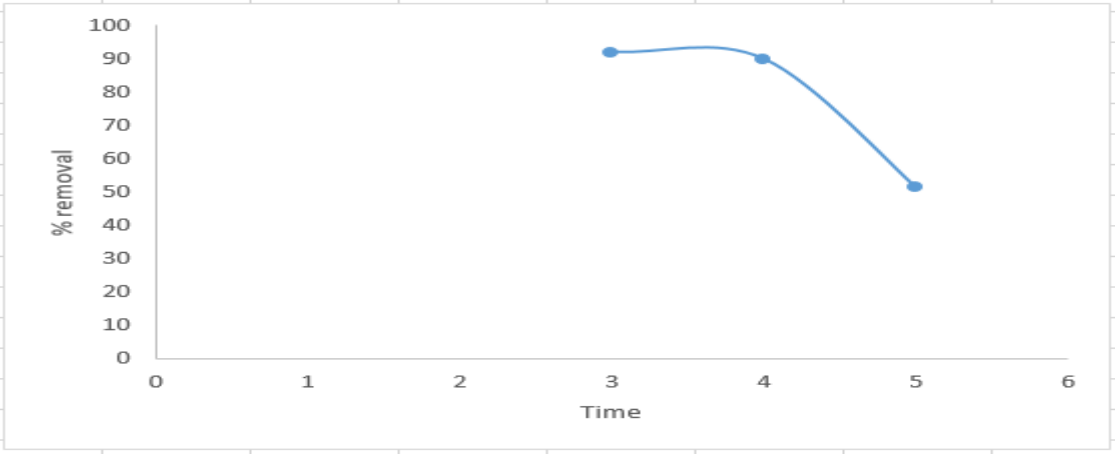

Fig.3.22. Graph showing the effect of size on Lead adsorption

From the aforementioned experiments, it's evident that the adsorption rate is influenced by the size of the sample; a larger sample size corresponds to a reduced adsorption effect. It's worth noting that a consistent amount of 5 mg of the nanomaterial was employed in all prior experiments for the adsorption process. Based on the comprehensive experimentation across all conditions, it's evident that the optimal temperature is 25°C, the most effective reaction time is 1 hour, and the optimal sample size is 3 ml.

3.6.3. Adsorption of Cadmium

Currently, both field and laboratory investigations have highlighted the roles of silicon (Si) in mitigating the toxicity of cadmium (Cd) and hindering its uptake by rice plants. These roles are primarily observed from two perspectives: Si either reduces the activity of cadmium in soil or hampers its movement and buildup within rice plants. Elevating the soil pH to 7 through Si application leads to a noteworthy reduction in available Cd, thereby causing the co-precipitation of Cd in forms like Cd(OH)2, Cd2(OH)3Cl, and CH6Br3Cd. [42].

The selection of the cadmium element was based on its elevated concentration in the measured samples and its potential impact on drinking water and living organisms. The highest concentration was intentionally selected to address purification needs. Employing optimal conditions, the nanomaterial was introduced for adsorption purposes. In this study, diverse parameters were taken into consideration for the adsorption of the aluminum element, including temperature, reaction time, and sample size.

Table 3.19. The effect of temperature

Temperatures ^{o}C	Conc.(ppb) before treatment	Conc.(ppb) After treatment	Removal efficiency(%)
20	26.7	5	81.27
25	26.7	16	40.07
30	26.7	14	47.56
35	26.7	9.5	64.41

In the provided table, the reaction time was set to 10 minutes, utilizing a sample volume of 5 ml while experimenting with various temperatures. Notably, the optimal adsorption of cadmium occurred at a temperature of 20 degrees Celsius when combined with the nanomaterial in our research. This outcome underscores the proficiency of the nanomaterial in effectively adsorbing cadmium.

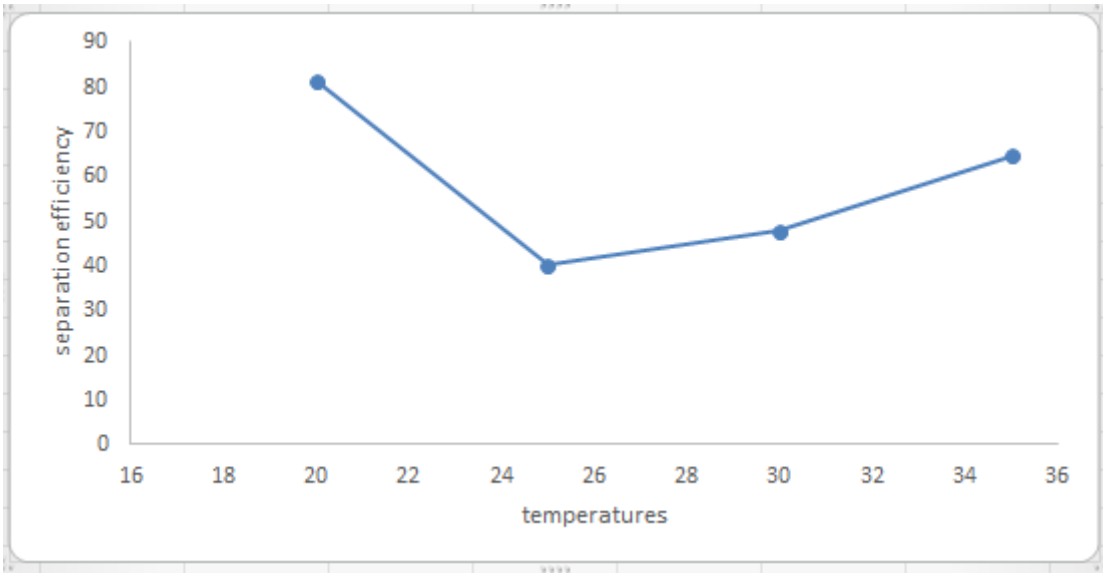

Fig. 3.23. The effect of temperature on cadmium adsorption

Table 3.20. The effect of contact time

Contact time	Conc.(ppb) before treatment	Conc.(ppb) After treatment	Removal efficiency (%)
5 min	26.7	13	51.31
10 min	26.7	9	66.29
30 min	26.7	5	81.27
1 hr.	26.7	4	85.01

By conducting experiments outlined in the provided table, with a consistent temperature of 20 °C and a sample volume of 5 mL, various temperatures were explored. Notably, within a one-hour timeframe, a highly effective adsorption process was observed for the cadmium element within the sample. This observation highlights the direct relationship between interaction time and adsorption efficiency, underscoring the remarkable efficacy of the nanomaterial utilized in our research.

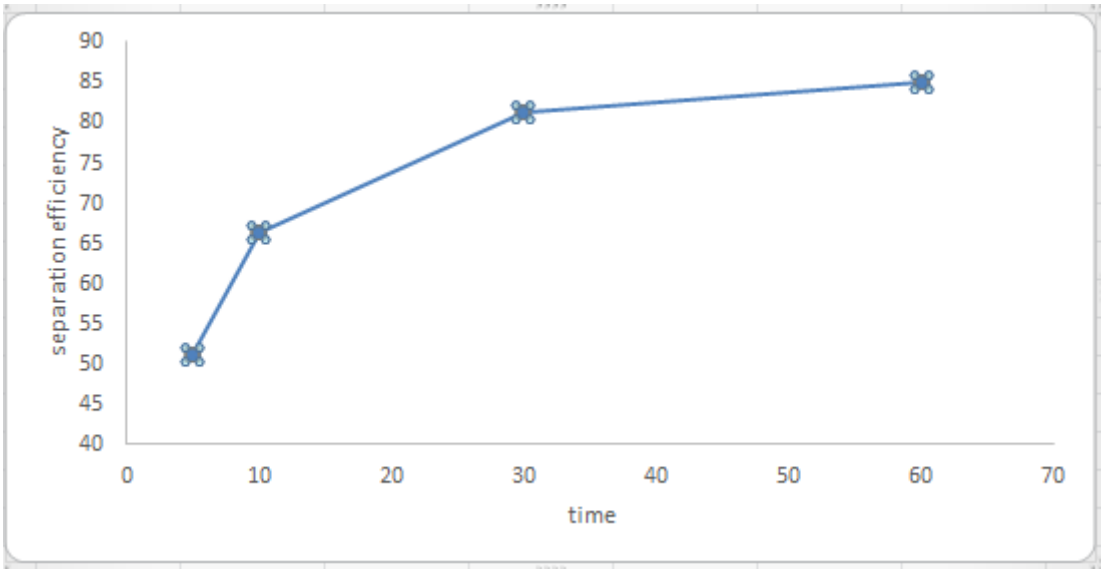

Fig. 3.24. The effect of reaction time on adsorption of cadmium

Table 3.21. The effect of sample size.

Size (mL)	Conc.(ppb) before treatment	Conc.(ppb) Aftertreatment	separation efficiency(%)
3	26.7	5.1	80.89
4	26.7	6.2	76.77
5	26.7	14	47.56

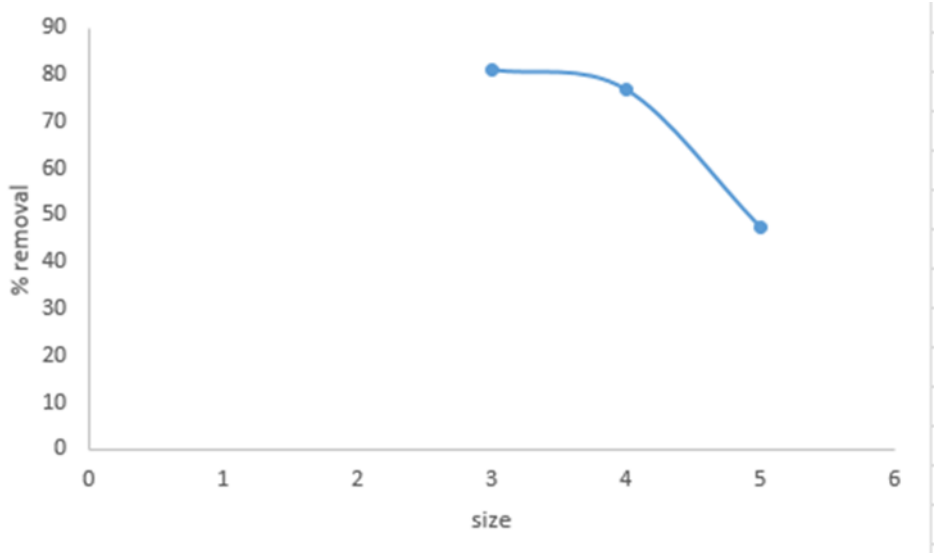

Fig.3.25. Graph showing the effect of size on cadmium adsorption

Based on the experiments detailed in the aforementioned table, conducted at a temperature of 20°C, a reaction time of 1 hour, and varying sample sizes, it was observed that with a sample size of 3 mL, a highly efficient adsorption process occurred for the cadmium element within the sample. This observation suggests a trend where smaller sample sizes lead to greater adsorption efficiency, indicating the high effectiveness of the employed nanomaterial in our research.

Furthermore, our research findings reveal that the synthesized nanomaterial demonstrates exceptional capability in adsorbing toxic heavy elements (aluminum, lead, and cadmium) at a notably high rate. The collective results point to the optimal adsorption conditions across all elements being a temperature of 25°C, a sample size of 3 mL, and a reaction time of 1 hour.

References

[1] W. S. Razzak, A. Al-taee, and A. A. Al-fanharawi, "Determination of some Heavy Metals Bioaccumulation in Water, Sediments, and Phragmites australis and Ceratophyllum demersum Plant in Euphrates River in Al-Samawa City/ Iraq," 2021.

[2] I. Ali *et al.*, "Polyaniline Modified CNTs and Graphene Nanocomposite for Removal of Lead and Zinc Metal Ions: Kinetics, Thermodynamics and Desorption Studies," *Molecules*, vol. 27, no. 17, 2022, doi: 10.3390/molecules27175623.

[3] I. Asati, AmbAli *et al.*, "Effect of Heavy Metals on Plants," *Int. J. Appl. or Innov. Eng. Manag.*, vol. 5, no. 03, pp. 56–66, 2016, doi: 10.13140/RG.2.2.27583.87204.

[4] I. Ismail and T. Moustafa, "Biosorption of heavy metals," *Heavy Met. Sources, Toxic. Remediat. Tech.*, no. October, pp. 131–174, 2016.

[5] T. saad Algarni and A. M. Al-Mohaimeed, "Water purification by adsorption of pigments or pollutants via metaloxide," *J. King Saud Univ. - Sci.*, vol. 34, no. 8, p. 102339, 2022, doi: 10.1016/j.jksus.2022.102339.

[6] Nishu and S. Kumar, "Smart and innovative nanotechnology applications for water purification," *Hybrid Adv.*, vol. 3, no. May, p. 100044, 2023, doi: 10.1016/j.hybadv.2023.100044.

[7] C. C. Kun, L. P. Yang, and M. C. Chang, "Adsorption of heavy metal ions by sodium chelating PAN fabrics," *Results Mater.*, vol. 16, no. November, p. 100344, 2022, doi: 10.1016/j.rinma.2022.100344.

[8] S. S. Alterary, A. A. Alshahrani, and S. A. Alsahli, "Fabrication of novel buckypaper metal oxide nano-catalysis glycerol carbonate/MWCNTs membrane for efficient removal of heavy metals," *Heliyon*, vol. 8, no. 12, 2022.

[9] G. Vignesh, P. Devendran, N. Nallamuthu, S. Sudhahar, P. S. Kumar, and M. K. Kumar, "Effects of nitrogen, sulphur, and temperature treatments on the spectral, structural, and electrochemical characteristics of graphene oxide for energy storage applications," *Carbon Trends*, vol. 11, no. December 2022, p. 100262, 2023, doi: 10.1016/j.cartre.2023.100262.

[10] O. Casabella-Font, M. Ponzelli, M. Papapanou, J. L. Balcazar, M. Pijuan, and J. Radjenovic, “Impact of graphene oxide addition on pharmaceuticals removal in anaerobic membrane bioreactor,” *Bioresour. Technol.*, vol. 383, no. May, p. 129252, 2023, doi: 10.1016/j.biortech.2023.129252.

[11] O. Casabella-Font, S. Zahedi, M. Gros, J. L. Balcazar, J. Radjenovic, and M. Pijuan, “Graphene oxide addition to anaerobic digestion of waste activated sludge: Impact on methane production and removal of emerging contaminants,” *Environ. Pollut.*, vol. 324, no. March, p. 121343, 2023, doi: 10.1016/j.envpol.2023.121343.

[12] A. Mulone, Z. Xia, and U. Klement, “Electrodeposition of FeW-graphene composites: Effect of graphene oxide concentration on microstructure, hardness and corrosion properties,” *FlatChem*, vol. 40, p. 100525, 2023, doi: 10.1016/j.flatc.2023.100525.

[13] R. Ghorbanpour Ghartavool, G. Reza Gordani, M. Reza Loghman Estarki, M. Tavoosi, M. Mazaheri Forushani, and E. Kiani, “Synthesis, microstructure, magnetic and electromagnetic behavior of graphene oxide/hexagonal barium ferrite aerogel nanocomposites within the frequency range of 1-18 GHz,” *Arab. J. Chem.*, p. 105099, 2023, doi: 10.1016/j.arabjc.2023.105099.

[14] M. Aghaee Malayeri, H. Koohestani, and M. Tajally, “Improving the properties of nickel/graphene oxide coated copper plate by changing the electroplating process conditions,” *Results Eng.*, vol. 18, no. March, p. 101167, 2023, doi: 10.1016/j.rineng.2023.101167.

[15] I. M. S. Al-Kadmy *et al.*, “Enhancing the anti-biofilm activity of novel keratinase isolated from Acinetobacter baumannii using Reduced Graphene oxide: A way to recycle feather waste pollution,” *Clean. Waste Syst.*, vol. 5, no. March, p. 100087, 2023, doi: 10.1016/j.clwas.2023.100087.

[16] J. Wang, H. Wang, S. Yang, G. Zhou, and Y. Mu, “Purification of heavy metal chromium in saturated sand by artificial freezing: Mechanism and method optimization,” *Res. Cold Arid Reg.*, vol. 14, no. 6, pp. 370–376, 2022, doi: 10.1016/j.rcar.2023.02.006.

[17] S. Kolathur, D. Khatiwada, and E. U. Khan, “Life cycle assessment and life cycle costing of a building-scale, solar-driven water purification system,” *Energy Nexus*, vol. 10, no. May, 2023, doi: 10.1016/j.nexus.2023.100208.

[18] Nishu and S. Kumar, “Smart and innovative nanotechnology applications for water purification,” *Hybrid Adv.*, vol. 3, no. March, p. 100044, 2023, doi: 10.1016/j.hybadv.2023.100044.

[19] Y. Zhai, G. Liu, and W. G. J. van der Meer, “One-Step Reverse Osmosis Based on Riverbank Filtration for Future Drinking Water Purification,” *Engineering*, vol. 9, pp. 27–34, 2022, doi: 10.1016/j.eng.2021.02.015.

[20] B. N. Huda, E. T. Wahyuni, and M. Mudasir, “Simultaneous Adsorption of Pb(II) and Cd(II) in the Presence of Mg(II) Ion Using Eco-Friendly Immobilized Dithizone on Coal Bottom Ash,” *South African J. Chem. Eng.*, vol. 45, no. November 2022, pp. 315–327, 2023, doi: 10.1016/j.sajce.2023.06.007.

[21] L. Velarde, M. S. Nabavi, E. Escalera, M. L. Antti, and F. Akhtar, “Adsorption of heavy metals on natural zeolites: A review,” *Chemosphere*, vol. 328, no. February, p. 138508, 2023, doi: 10.1016/j.chemosphere.2023.138508.

[22] S. Nezami, A. Ghaemi, and T. Yousefi, “Application of titanium carbide/nitride (MXene)-based NPs in adsorption of radionuclides and heavy metal ions for wastewater remediation: A review,” *Case Stud. Chem. Environ. Eng.*, vol. 7, no. January, p. 100326, 2023, doi: 10.1016/j.cscee.2023.100326.

[23] Y. Wang, Y. Wang, Y. Wang, and J. Liu, “Facial preparation of covalent modified reduced graphene oxide/polyaniline composite and its stable-enhanced electrochemical performance,” *Heliyon*, vol. 9, no. 1, p. e13002, 2023, doi: 10.1016/j.heliyon.2023.e13002.

[24] M. Mohammadi, S. Sabbaghi, M. Binazadeh, S. Ghaedi, and H. Rajabi, “Type-1 α-Fe2O3/TiO2 photocatalytic degradation of tetracycline from wastewater using CCD-based RSM optimization,” *Chemosphere*, vol. 336, no. May, p. 139311, 2023, doi: 10.1016/j.chemosphere.2023.139311.

[25] B. A. M. Babakir, L. I. Abd Ali, and H. K. Ismail, “Rapid removal of anionic organic dye from contaminated water using a poly(3-aminobenzoic acid/graphene oxide/cobalt ferrite) nanocomposite low-cost adsorbent via adsorption techniques,” *Arab. J. Chem.*, vol. 15, no. 12, p. 104318, 2022, doi: 10.1016/j.arabjc.2022.104318.

[26] M. M. Zankana, S. M. Al-dalawy, and A. A. Barzinjy, “Synthesis and characterization of bio-nanocomposites : Functionalization of graphene oxide with a biocompatible amino acid,” *Hybrid Adv.*, vol. 3, no. June, p. 100070, 2023, doi: 10.1016/j.hybadv.2023.100070.

[27] G. Vignesh, P. Devendran, N. Nallamuthu, S. Sudhahar, P. S. Kumar, and M. K. Kumar, “Effects of nitrogen, sulphur, and temperature treatments on the spectral, structural, and electrochemical characteristics of graphene oxide for energy storage applications,” *Carbon Trends*, vol. 11, p. 100262, 2023.

[28] M. Azriouil *et al.*, “Chemically reduced graphene oxide sheets for voltammetric determination of ciprofloxacin in biological fluids and pharmaceutical formulations,” *J. Hazard. Mater. Adv.*, vol. 11, no. May, p. 100356, 2023, doi: 10.1016/j.hazadv.2023.100356.

[29] R. M. Hameed, A. Al-haddad, and A. K. H. Albarazanchi, “Facile transformation of graphene oxide nanospheres based on AAO template,” *Kuwait J. Sci.*, no. October 2022, 2023, doi: 10.1016/j.kjs.2023.08.002.

[130] Y. Wang, Y. Wang, Y. Wang, and J. Liu, “Facial preparation of covalent modified reduced graphene oxide/polyaniline composite and its stable-enhanced electrochemical performance,” *Heliyon*, vol. 9, no. 1, p. e13002, 2023, doi: 10.1016/j.heliyon.2023.e13002.

[31] M. Mohammadi, S. Sabbaghi, M. Binazadeh, S. Ghaedi, and H. Rajabi, “Type-1 α-Fe2O3/TiO2 photocatalytic degradation of tetracycline from wastewater using CCD-based RSM optimization,” *Chemosphere*, vol. 336, no. May, p. 139311, 2023, doi: 10.1016/j.chemosphere.2023.139311.

[32] P. Praipipat, P. Ngamsurach, and K. Pratumkaew, “The synthesis, characterizations, and lead adsorption studies of chicken eggshell powder and chicken eggshell powder-doped

iron (III) oxide-hydroxide," *Arab. J. Chem.*, vol. 16, no. 5, p. 104640, 2023, doi: 10.1016/j.arabjc.2023.104640.

[33] P. Praipipat, P. Ngamsurach, and K. Pratumkaew, "The synthesis, characterizations, and lead adsorption studies of chicken eggshell powder and chicken eggshell powder-doped iron (III) oxide-hydroxide," *Arab. J. Chem.*, vol. 16, no. 5, p. 104640, 2023.

[34] Q. Ji, L. Han, T. Zhang, X. Xia, and X. Xiang, "α-Linolenic acid alleviates aluminum toxicity in RAW264. 7 cells by antioxidative and anti-inflammatory effects," *Arab. J. Chem.*, vol. 16, no. 8, p. 104931, 2023.

[35] G. A. V Price *et al.*, "Natural organic matter source, concentration, and pH influences the toxicity of zinc to a freshwater microalga," *Environ. Pollut.*, vol. 318, p. 120797, 2023.

[36] L. Kang, M. Mucci, J. Fang, and M. Lürling, "New is not always better: Toxicity of novel copper based algaecides to Daphnia magna," *Ecotoxicol. Environ. Saf.*, vol. 241, no. March, p. 113817, 2022, doi: 10.1016/j.ecoenv.2022.113817.

[37] S. M. Ramraj, A. Kubaib, P. M. Imran, and M. K. Thirupathy, "Utilizing Sida Acuta leaves for low-cost adsorption of chromium (VI) heavy metal with activated charcoal," *J. Hazard. Mater. Adv.*, vol. 11, no. June, 2023, doi: 10.1016/j.hazadv.2023.100338.

[38] R. Revathy, T. Sajini, C. Augustine, and N. Joseph, "Iron-based magnetic nanomaterials: Sustainable approaches of synthesis and applications," *Results Eng.*, vol. 18, no. April, p. 101114, 2023, doi: 10.1016/j.rineng.2023.101114.

[39] B. A. M. Babakir, L. I. Abd Ali, and H. K. Ismail, "Rapid removal of anionic organic dye from contaminated water using a poly(3-aminobenzoic acid/graphene oxide/cobalt ferrite) nanocomposite low-cost adsorbent via adsorption techniques," *Arab. J. Chem.*, vol. 15, no. 12, p. 104318, 2022, doi: 10.1016/j.arabjc.2022.104318.

[40] M. M. Zankana, S. M. Al-dalawy, and A. A. Barzinjy, "Synthesis and characterization of bio-nanocomposites : Functionalization of graphene oxide with a biocompatible amino acid," *Hybrid Adv.*, vol. 3, no. June, p. 100070, 2023, doi: 10.1016/j.hybadv.2023.100070.

[41] G. Vignesh, P. Devendran, N. Nallamuthu, S. Sudhahar, P. S. Kumar, and M. K. Kumar, "Effects of nitrogen, sulphur, and temperature treatments on the spectral, structural, and electrochemical characteristics of graphene oxide for energy storage applications," *Carbon Trends*, vol. 11, p. 100262, 2023.

[42] M. Azriouil *et al.*, "Chemically reduced graphene oxide sheets for voltammetric determination of ciprofloxacin in biological fluids and pharmaceutical formulations," *J.*